Boundary spectrum in the sine-Gordon model with Dirichlet boundary conditions

2000 J. Phys. A: Math. Gen. 33 9065

(http://iopscience.iop.org/0305-4470/33/49/304)

J. Phys. A: Math. Gen. **33** (2000) 9065–9093. Printed in the UK PII: S0305-4470(00)16597-7

Boundary spectrum in the sine–Gordon model with Dirichlet boundary conditions

Peter Mattsson† and Patrick Dorey

Department of Mathematical Sciences, University of Durham, Durham DH1 3LE, UK

E-mail: P.A.Mattsson@Open.ac.uk

Received 23 August 2000

Abstract. We find the spectrum of boundary bound states for the sine–Gordon model with Dirichlet boundary conditions, closing the bootstrap and providing a complete description of all the poles in the boundary reflection factors. The boundary Coleman–Thun mechanism plays an important role in the analysis. Two basic lemmas are introduced which should hold for any $(1+1)$-dimensional boundary field theory, allowing the general method to be applied to other models.

1. Introduction

Integrable quantum field theories in two dimensions can be restricted from the whole line by certain boundary conditions while still preserving their integrability [1]. As well as being of theoretical interest, these models have interesting physical applications, for example, to impurity problems in an interacting one-dimensional (1D) electron gas [2] or edge excitations in fractional quantum Hall states [3, 4]. (A recent review can be found in [5].)

One such theory is the sine–Gordon model, which has the bulk action

$$\mathcal{A}_{SG} = \int_{-\infty}^{\infty} \mathrm{d}x \int_{-\infty}^{\infty} \mathrm{d}t \left[\tfrac{1}{2}(\partial_\mu \varphi)^2 - \frac{m_0^2}{\beta^2}(\cos(\beta\varphi) - 1) \right] \tag{1}$$

on the full line, where $\varphi(x, t)$ is a scalar field and β is a dimensionless coupling constant. It was argued in [1] that this could be restricted to the half-line $x \in (-\infty, 0]$, while still preserving integrability by adding a 'boundary action' term

$$-\int_{-\infty}^{\infty} \mathrm{d}t\, M \cos\left[\tfrac{1}{2}\beta(\varphi_B - \varphi_0)\right] \tag{2}$$

where M and φ_0 are free parameters, and $\varphi_B(t) = \varphi(x, t)|_{x=0}$. In addition to the usual bulk bound states, in general this also presents us with a complicated spectrum of boundary bound states. This aspect was mentioned briefly in [1, 6], and investigated in more detail in [7]. However, in none of these works was a full explanation of all poles achieved. In this paper we return to the problem, and find that the full story appears to involve a much richer structure of boundary bound states than has previously been suggested. An important feature of our analysis, not taken into account in the earlier works, is the so-called boundary Coleman–Thun mechanism [8]. After a brief description of the boundary sine–Gordon model in section 2, this

† Present address: Media Development, Open University, Walton Hall, Milton Keynes MK7 6AA, UK.

0305-4470/00/499065+29$30.00

mechanism is reviewed in section 3. In the course of the section we also develop a couple of useful lemmas, which simplify the subsequent discussions considerably.

We will restrict ourselves to the case of Dirichlet boundary conditions, which simply fixes the value of the field at the boundary to $\varphi(x = 0, t) = \varphi_0$ for all time. This corresponds to taking $M \to \infty$ above. After an initial discussion in section 4, in section 5 we give a complete analysis of a particular example. This serves to show many of the features of the bound state structure, and is a useful warm-up to the discussion of the general case in section 6. Finally, we gather together our conclusions in section 7.

2. The reflection factors

2.1. The theory in the bulk

We begin with a summary of the theory in the bulk, mainly to set up the notation. Further details can be found in the review [9]. The bulk sine–Gordon model is known to be integrable at both the classical and the quantum levels [10]. The theory has an infinite number of degenerate vacua, with the discrete symmetry $\varphi \to \varphi + \frac{2\pi}{\beta}m$, with $m \in \mathbb{Z}$. The particle spectrum consists of a soliton (A) and an antisoliton ($\overline{A}$)—both of which interpolate between neighbouring vacua—and a number of soliton–antisoliton bound states ('breathers') B_n, $n = 1, 2, \ldots, < \lambda$, where

$$\lambda = \frac{8\pi}{\beta^2} - 1. \tag{3}$$

The soliton (antisoliton) has a topological charge of 1 (-1), while the breathers are neutral. The soliton and antisoliton both have the same mass, which we shall call m_s, while the mass of the nth breather B_n is $m_n = 2m_s \sin\left(\frac{n\pi}{2\lambda}\right)$.

The integrability of the theory means that particle production is forbidden, and all scattering is factorizable—the amplitude for any scattering process can be reduced to a product of two-particle amplitudes. In addition, charge, parity and time-reversal (C, P and T) symmetry holds for the bulk theory. If we denote the soliton S-matrix as $S_{cd}^{ab}(\theta)$ for rapidity θ, with a, b, c, d taking the value + ($-$) if the particle is a soliton (antisoliton), the non-zero scattering amplitudes are $S_{++}^{++}(\theta) = S_{--}^{--}(\theta) = a(\theta)$ (soliton–soliton or antisoliton–antisoliton scattering), $S_{+-}^{+-}(\theta) = S_{-+}^{-+}(\theta) = b(\theta)$ (soliton–antisoliton transmission), and $S_{-+}^{+-}(\theta) = S_{+-}^{-+}(\theta) = c(\theta)$ (soliton–antisoliton reflection). Explicitly,

$$\begin{aligned} a(\theta) &= \sin[\lambda(\pi - u)]\rho(u) \\ b(\theta) &= \sin(\lambda u)\rho(u) \\ c(\theta) &= \sin(\lambda\pi)\rho(u) \end{aligned} \tag{4}$$

where $u = -\mathrm{i}\theta$ and

$$\rho(u) = \frac{1}{\sin(\lambda(u-\pi))}\prod_{l=1}^{\infty}\left[\frac{\Gamma\left((2l-2)\lambda - \lambda u/\pi\right)\Gamma\left(1+2l\lambda - \lambda u/\pi\right)}{\Gamma\left((2l-1)\lambda - \lambda u/\pi\right)\Gamma\left(1+(2l-1)\lambda - \lambda u/\pi\right)}\Big/(u \to -u)\right]. \tag{5}$$

As pointed out in [11], this factor can also be written in terms of Barnes' diperiodic sine function $S_2(x|\omega_1, \omega_2)$ [12, 13]. This is a meromorphic function parametrized by the pair of 'quasiperiods' (ω_1, ω_2), with poles and zeros at the following points:

$$\text{poles:} \quad x = n_1\,\omega_1 + n_2\,\omega_2 \qquad (n_1, n_2 = 1, 2, \ldots) \tag{6}$$

$$\text{zeros:} \quad x = m_1\,\omega_1 + m_2\,\omega_2 \qquad (m_1, m_2 = 0, -1, -2\ldots). \tag{7}$$

In terms of this function,

$$\rho(u) = \frac{1}{\sin(\lambda(u-\pi))} \frac{S_2\,(\pi - u\,|\pi/\lambda, 2\pi\,)\,S_2\,(u\,|\pi/\lambda, 2\pi\,)}{S_2\,(\pi + u\,|\pi/\lambda, 2\pi\,)\,S_2\,(-u\,|\pi/\lambda, 2\pi\,)}. \tag{8}$$

The amplitudes $b(\theta)$ and $c(\theta)$ have simple poles at $\theta = \mathrm{i}\left(\pi - \frac{n\pi}{\lambda}\right)$, $n = 1, 2, \ldots, < \lambda$, which can be attributed to the creation of B_n in the forward channel. There are also poles at $\theta = \frac{\mathrm{i}\pi n}{\lambda}$ in $a(\theta)$ and $b(\theta)$ corresponding to the same process in the cross channel. Since all poles that we will be discussing, both in the bulk and at the boundary, occur at imaginary rapidities, from now on we will use the variable $u = -\mathrm{i}\theta$ and always work in terms of purely imaginary rapidities.

2.2. Solitonic ground state reflection factors

The general integral boundary condition found in [1] does not conserve topological charge, so in principle four solitonic boundary reflection factors need to be introduced, as well as a set of breather reflection factors. The solitonic factors which we quote here were given in [1], while breather factors can be found in [6]. The reflection factors for the sine–Gordon solitons off the boundary ground state will be denoted by $P_\pm(u)$ (a soliton or antisoliton, incident on the boundary, is reflected back unchanged) and $Q_\pm(u)$ (a soliton is reflected back as an antisoliton, or vice versa). In the Dirichlet case, topological charge is conserved and so $Q_\pm = 0$. The remaining factors can be written as†

$$P^{\pm}(u) = R_0(u) \prod_{l=1}^{\infty} \left[\frac{\Gamma\left(\frac{1}{2} + 2l\lambda \pm \xi/\pi + \lambda u/\pi\right) \Gamma\left(\frac{1}{2} + (2l-2)\lambda \mp \xi/\pi + \lambda u/\pi\right)}{\Gamma\left(\frac{1}{2} + (2l-1)\lambda + \xi/\pi + \lambda u/\pi\right) \Gamma\left(\frac{1}{2} + (2l-1)\lambda - \xi/\pi + \lambda u/\pi\right)} \Big/ (u \to -u) \right] \tag{9}$$

where

$$R_0(u) = \prod_{k=1}^{\infty} \left[\frac{\Gamma\,(1 + \lambda(4k-4) - 2\lambda u/\pi)\,\Gamma\,(4\lambda k - 2\lambda u/\pi)}{\Gamma\,(\lambda(4k-3) - 2\lambda u/\pi)\,\Gamma\,(1 + \lambda(4k-1) - 2\lambda u/\pi)} \Big/ (u \to -u) \right] \tag{10}$$

and $\xi = \frac{4\pi\varphi_0}{\beta}$. These factors can again be written in terms of Barnes' multiperiodic functions, as

$$P^{\pm}(u) = R_0(u) \frac{S_2\,(\pi/2\lambda \mp \xi/\lambda + \pi + u\,|\pi/\lambda, 2\pi\,)\,S_2\,(\pi/2\lambda \mp \xi/\lambda - u\,|\pi/\lambda, 2\pi\,)}{S_2\,(\pi/2\lambda \mp \xi/\lambda + \pi - u\,|\pi/\lambda, 2\pi\,)\,S_2\,(\pi/2\lambda \mp \xi/\lambda + u\,|\pi/\lambda, 2\pi\,)} \tag{11}$$

with

$$R_0(u) = \frac{S_2\,(\pi/2 - u\,|\pi/2\lambda, 2\pi\,)\,S_2\,(\pi/2\lambda + u\,|\pi/2\lambda, 2\pi\,)}{S_2\,(\pi/2 + u\,|\pi/2\lambda, 2\pi\,)\,S_2\,(\pi/2\lambda - u\,|\pi/2\lambda, 2\pi\,)}. \tag{12}$$

The theory is invariant under $\varphi_0 \to \varphi_0 + \frac{2\pi}{\beta}$, and also under the simultaneous transformations $\varphi_0 \to -\varphi_0$ and soliton $\to$ antisoliton. Introducing the boundary breaks the degeneracy of the bulk vacua, and selects the lower line in figure 1 as the lowest-energy state, with the upper line as the first excited state. Continuing φ_0 through $\frac{\pi}{\beta}$ thus simply interchanges the roles of these two states, and selects the upper one as the ground state.

In light of this, we are free to choose ξ to be in the interval

$$0 < \xi < \frac{4\pi^2}{\beta^2} = \frac{\pi(\lambda+1)}{2}. \tag{13}$$

† Note that there is a small error in Ghoshal and Zamolodchikov's formula (5.23) for σ, where the denominator should read $\Pi(x, \pi/2)\Pi(-x, \pi/2)\Pi(x, -\pi/2)\Pi(-x, -\pi/2)$. We are grateful to Subir Ghoshal for informing us of the corrected version.

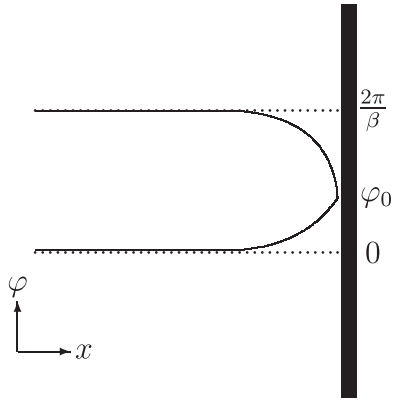

Figure 1. Vacuum structure.

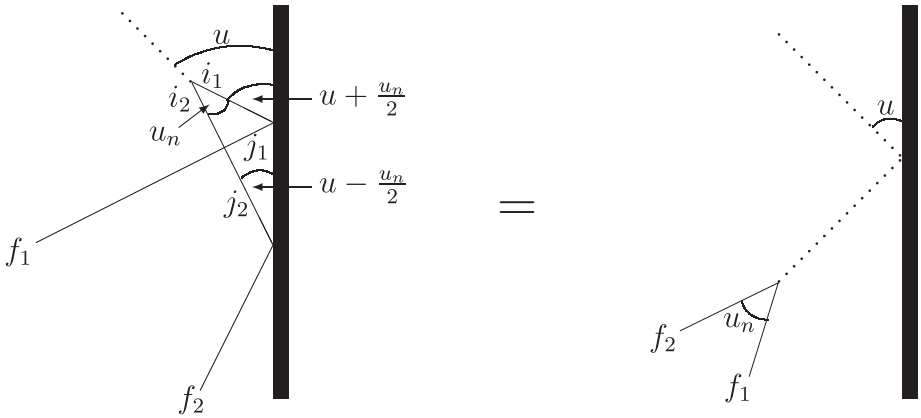

Figure 2. Breather bootstrap.

Note that the topological charge of the ground state is no longer zero, as in the bulk model, but

$$q = \frac{\beta}{2\pi}\int_{-\infty}^{0} \mathrm{d}x \frac{\partial}{\partial x}\varphi(x,t) = \frac{\beta}{2\pi}[\varphi(0,t) - \varphi(-\infty,t)] = \frac{\beta\varphi_0}{2\pi} \tag{14}$$

with the charge of the first excited state being $1 - \frac{\beta\varphi_0}{2\pi}$. We will find that all the boundary states have one of these charges, so, for convenience, we shall designate them simply as 0 and 1, respectively.

2.3. Breather ground state reflection factors

For the breather sector, Ghoshal [6] obtained the relevant reflection factors, $R^n_{|0\rangle}(u)$ for breather n and boundary ground state $|0\rangle$, from the solitonic reflection factors using the general boundary bootstrap equation [1, 14]

$$f^n_{i_1 i_2} R^{i_1}_{j_1|x\rangle}\left(u + \frac{u_n}{2}\right) S^{i_2 j_1}_{j_2 f_1}(2u) R^{j_2}_{f_2|x\rangle}\left(u - \frac{u_n}{2}\right) = f^n_{f_1 f_2} R^n_{|x\rangle}(u) \tag{15}$$

where $u_n = \pi - \frac{n\pi}{\lambda}$, and the $R^a_{b|x\rangle}(u)$ are the solitonic reflection factors, such that $R^+_{-|x\rangle}(u)$ is the factor for a soliton to be reflected back as an antisoliton and so on. The f^n_{ab} are the bulk vertices for the creation of breather n from (anti)solitons a and b. These obey $f^n_{+-} = (-1)^n f^n_{-+}$. The bootstrap is illustrated in figure 2.

In the Dirichlet case, with topological charge conserved, the bootstrap equation reduces to

$$f^n_{i_1 i_2} P^{i_1}_{|x\rangle}\left(u+\frac{u_n}{2}\right) S^{i_2 i_1}_{f_2 f_1}(2u) P^{f_2}_{|x\rangle}\left(u-\frac{u_n}{2}\right) = f^n_{f_1 f_2} R^n_{|x\rangle}(u). \tag{16}$$

Ghoshal found that, for the boundary ground state, the breather reflection factors were

$$R^n_{|0\rangle}(u) = R^{(n)}_0(u) R^{(n)}_1(u) \tag{17}$$

where

$$R^{(n)}_0(u) = \frac{\frac{1}{2}(n/2\lambda+1)}{\left(n/2\lambda+\frac{3}{2}\right)} \prod_{l=1}^{n-1} \frac{(l/2\lambda)\,(l/2\lambda+1)}{\left(l/2\lambda+\frac{3}{2}\right)^2} \tag{18}$$

and

$$R^{(n)}_1(u) = \prod_{l=(1-n)/2}^{(n-1)/2} \frac{\left(\xi/\lambda\pi - \frac{1}{2} + l/2\lambda\right)}{\left(\xi/\lambda\pi + \frac{1}{2} + l/2\lambda\right)}. \tag{19}$$

This makes use of the notation

$$(x) = \frac{\sinh(\theta/2 + \mathrm{i}\pi x/2)}{\sinh(\theta/2 - \mathrm{i}\pi x/2)} \tag{20}$$

which will also be helpful later.

3. The boundary Coleman–Thun mechanism

In this section we will discuss some general features of the pole analysis of boundary reflection factors, in preparation for the specific case of the sine–Gordon model. The main aim is to establish a couple of lemmas which will simplify the subsequent discussion. We begin by recalling the story in the bulk.

An initially mysterious feature of the sine–Gordon S-matrix was the presence of a number of double poles in the breather scattering amplitudes. At first it was thought that these might be related to the integrability of the model, and it was only with the work of Coleman and Thun [15] that it was realized that they had a 'prosaic' origin as anomalous threshold poles, and could be explained using standard field-theoretical ideas. Studies of affine Toda field theories [16–19] returned to this topic, and it proved possible, in certain cases, to confirm the scenario of Coleman and Thun through standard, albeit elaborate, perturbative calculations [18].

One element of Coleman and Thun's analysis was the observation that in $1+1$ dimensions sometimes even simple poles have complicated explanations, as anomalous thresholds. This breaks the usual association of every simple S-matrix pole with a bound state in either the forward or the crossed channel. The same mechanism is at work in the S-matrices of non-self-dual affine Toda field theories [19], as was pointed out in [20]. This material is reviewed at greater length in [21]; here, we are more interested in what can occur when a boundary is also involved. This was discussed in [8] via a particularly simple example, the boundary scaling Lee–Yang model, for which the spectrum of boundary bound states had previously been found by other means [22]. It was found that the Coleman–Thun mechanism did indeed play a role, there being a number of simple poles in the reflection factors at locations which did not correspond to boundary bound states, but which rather could be explained through on-shell (anomalous threshold) diagrams for multiple rescattering processes involving the boundary. Further work, applying the method to affine Toda field theories, can be found in [23]. It is important to note that, both in the bulk and at the boundary, an anomalous threshold diagram would normally lead to a pole of order greater than one. To match a simple pole, this order

must be reduced somehow, and in [8, 23] this was always achieved by one or more 'internal' reflection factors having zeros exactly at the point where the diagram went on-shell. Here, we will see both this mechanism of order reduction (which mimics that seen in bulk affine Toda theories [20]) and cancellations between different diagrams, i.e. closer to the original situation discussed by Coleman and Thun [15].

One difficulty, which is especially serious in cases when the spectrum of boundary bound states is not known *a priori*, is the greatly increased complexity of the on-shell diagrams once a boundary is involved. This makes it hard to be sure that any given pole really does correspond to a new boundary bound state. In the bulk, a simple geometrical argument shows that poles in the S-matrix elements of the lightest particle can never be explained by a Coleman–Thun mechanism, and so must always be due to bound states [17]. We wish to find analogous criteria for the boundary situation. To this end, the following two lemmas turn out to be useful. Suppose the incoming particle is of type a, and that its reflection factor has a simple pole at $\theta = \mathrm{i}u$.

Lemma 1. *Let* $\overline{U}_a = \min_{b,c}\left(\pi - U_{ab}^{c}\right)$. *If* $u < \overline{U}_a$, *then the pole at* iu *cannot be explained by a Coleman–Thun mechanism, and so must correspond to the binding of particle a to the boundary, either before or after crossing the outgoing particle.*

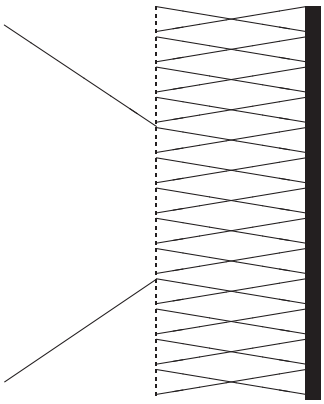

Figure 3. General process with incoming particles uncrossed.

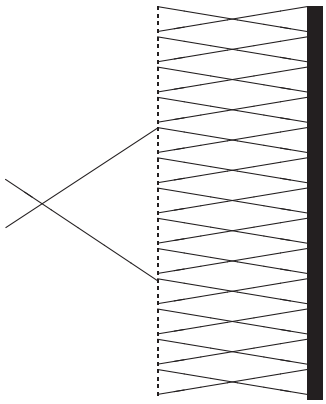

Figure 4. General process with incoming particles crossed.

Proof. All processes must take the form shown in figure 3 or the crossed version shown in figure 4. Conservation of momentum demands that all rescattering must take place within the hatched region, which is drawn from the furthest point from the boundary where either the incoming or outgoing particle undergoes any interaction. If neither particle decays, we simply have a diagram of the form of figure 7(b) or figure 7(c). Otherwise, momentum conservation requires that neither product of the particle which decays on the boundary of the hatched region has a trajectory which takes it outside that region. Fixing the notation by figure 5 (with angles U_{ac}^{b} and U_{ab}^{c} defined correspondingly), this reduces to demanding $\pi - U_{ab}^{c} \leqslant u \leqslant U_{ac}^{b}$. If we introduce $\overline{U}_a$ then we must have $\overline{U}_a \leqslant u \leqslant \pi - \overline{U}_a$ (i.e. just $u \geqslant \overline{U}_a$, as $u \leqslant \frac{\pi}{2}$). Thus, if $u < \overline{U}_a$, then the only possible explanations for the pole are figures 7(b) and 7(c). □

Lemma 2. *If the boundary is in its ground state, then lemma 1 can be strengthened, requiring that the incoming particle bind to the boundary if* u *is outside the range* $\overline{U}_a < u < \frac{\pi}{2} - \overline{U}_a$. *In addition, if* $\min_{b,c} U_{bc}^{a} > \frac{\pi}{2}$, *the incoming particle must always bind to the boundary.*

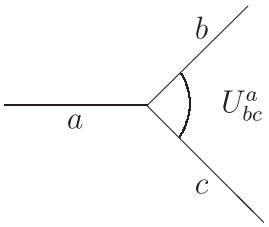

Figure 5. Decay process.

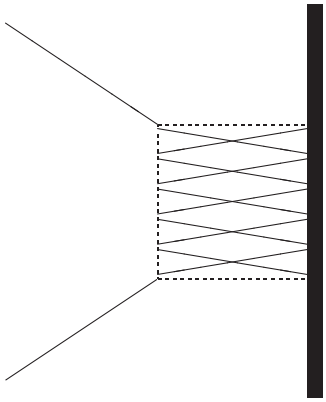

Figure 6. General ground state process.

Proof. With the boundary in its ground state, all rescattering must take place in the area shown in figure 6. Reasoning as before but demanding that both product particles be emitted into this more restricted region, we find $\pi - U^c_{ab} \leqslant u \leqslant U^b_{ac} - \frac{\pi}{2}$, or $\overline{U}_a \leqslant u \leqslant \frac{\pi}{2} - \overline{U}_a$. In addition, both particles b, c must be emitted into an angle of $\frac{\pi}{2}$, so $U^a_{bc} < \frac{\pi}{2}$ for at least one pair of particles b, c. If either of these conditions are violated, then the incoming particle must bind to the boundary. □

These two results, between them, will allow the spectrum of the sine–Gordon model with Dirichlet boundary conditions to be fixed completely, provided it is assumed that no pole corresponds to the creation of a boundary state if it has an alternative (Coleman–Thun) explanation.

For the problem under discussion, writing the rapidity bounds $\overline{U}_a$ as $\overline{U}_{+(-)}$ for the soliton (antisoliton) and as $\overline{U}_n$ for the B_n, we have

$$\begin{aligned} \overline{U}_{\pm} &= \frac{\pi}{2} - \frac{n_{\max}\pi}{2\lambda} \\ \overline{U}_n &= \pi/2\lambda \qquad n \neq n_{\max} \\ \overline{U}_{n_{\max}} &= \frac{\pi}{2} - \frac{n_{\max}\pi}{2\lambda} \end{aligned} \tag{21}$$

where $B_{n_{\max}}$ is the highest-numbered breather present in the model. To derive these results, note that a soliton (antisoliton) can only decay into an antisoliton (soliton) and a breather (with vertex $U^{\pm}_{\mp n} = \frac{\pi}{2} + \frac{n\pi}{2\lambda}$). A breather can either decay into a soliton–antisoliton pair ($U^n_{+-} = \pi - \frac{n\pi}{\lambda}$) or a pair of breathers ($U^l_{nm} = \pi - \frac{l\pi}{2\lambda}$ with $n = m + l$ or $m = n + l$, or $U^l_{nm} = \frac{\pi(n+m)}{2\lambda}$ with $l = n + m$).

These restrictions can also be combined to produce a stronger version of lemma 1 when the incoming particle is a soliton. If $\overline{U}_+ < u < \frac{\pi}{\lambda}$, decay within the hatched region is only possible into the topmost breather and an antisoliton. One or other of these particles will be heading away from the centre of the diagram. If the process in uncrossed, as in figure 3, the breather will be created heading towards the centre of the diagram, and the antisoliton away (we are being somewhat cavalier with the direction of time; this should be considered as a purely geometric argument). The antisoliton must itself obey our lemmas; if in any further decay before it reaches the boundary one of the decay products is heading away from the boundary, then there would be no way to close the diagram while conserving momentum at

every vertex. For a crossed process (figure 4) the breather is the outermost particle, and is again restricted in its decay by our lemmas for the same reason.

The antisoliton created by the uncrossed process heads for the boundary with a rapidity less than $\overline{U}_-$ and so, by lemma 1, may not decay. By the same token, the breather of the crossed process cannot decay either, so, if the initial soliton is not to form a bound state, the only possible alternative processes are figures B2 and B3. If these are found not to occur (for example, if the necessary boundary vertices are not present) then the pole must correspond to a bound state for any $u < \frac{\pi}{\lambda}$.

4. Initial pole analysis

4.1. Solitonic ground state factors

The $R_0(u)$ factor is insensitive to the boundary parameters, and so all of its poles should be explicable in terms of the bulk. The only poles are at $u = \frac{N\pi}{2\lambda}$, where $N = 1, 2, 3, \ldots$, with no zeros. These can be explained by the creation of a breather which is incident perpendicularly on the boundary, as shown in figure 7(a). Here, as in all subsequent diagrams, the time axis points up the page, and the x-axis points to the right. Solitons and antisolitons are drawn as full lines, while breathers are drawn as dotted lines.

Turning now to ξ-dependent poles and zeros, we find zeros at

$$u = -\frac{\xi}{\lambda} + \frac{(2n+1)\pi}{2\lambda} \tag{22}$$

where $n = 0, 1, 2, \ldots$, for P^+, and at the same rapidities but with $\xi \to -\xi$ for P^-. There are also poles in P^+ only at $u = \nu_n$, with

$$\nu_n = \frac{\xi}{\lambda} - \frac{(2n+1)\pi}{2\lambda}. \tag{23}$$

A soliton can only decay into an antisoliton and a breather, with a rapidity difference between the two of $\frac{\pi}{2} + \frac{b\pi}{2\lambda}$ for breather b. Thus, by lemma 2, all of these poles must correspond to bound states, as shown in figure 7(b). For reasons which will become clear in a moment, we shall depart from the convention of [7] and, rather than labelling the state corresponding to pole ν_n as β_n, will label it according to topological charge and n as $|1; n\rangle$.

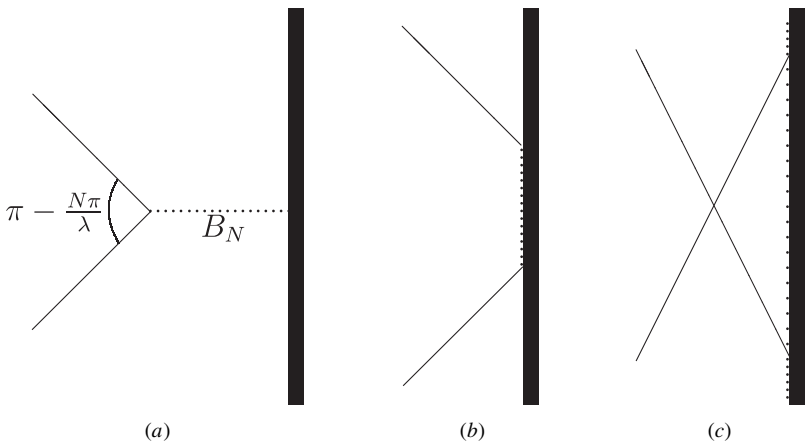

Figure 7. (a) ξ-independent pole. (b) Bound state. (c) Crossed process.

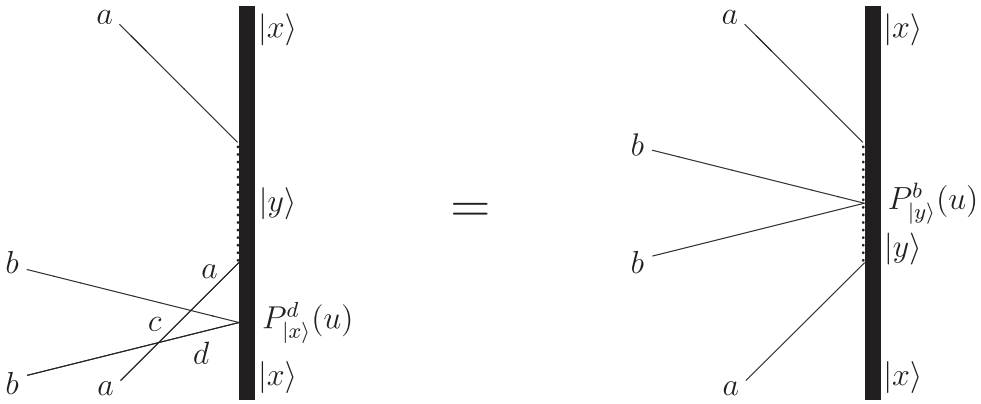

Figure 8. Boundary bound-state bootstrap.

4.2. Solitonic excited state reflection factors

Using the boundary bootstrap equations given in [1], which come from considering figure 8, solitonic reflection factors can be calculated for this first set of bound states. In our case, these equations read

$$P^b_{|y\rangle}(u) = \sum_{c,d} P^d_{|x\rangle}(u) S^{ab}_{cd}(u - \alpha^y_{ax}) S^{dc}_{ba}(u + \alpha^y_{ax}) \tag{24}$$

where a, b, c and d take the values + or − and α^y_{ax} is the (imaginary) rapidity of the pole at which particle a binds to boundary state $|x\rangle$ to give state $|y\rangle$. The mass of state $|y\rangle$ (m_y) is given by

$$m_y = m_x + m_s \cos \alpha^y_{ax}. \tag{25}$$

Taking x to be the ground state $|0\rangle$ and y to be one of the set of excited states $|1; n\rangle$, this gives

$$\begin{aligned} P^+_{|1;n\rangle}(u) &= P^+_{|0\rangle}(u)\, a(u - \nu_n)\, a(u + \nu_n) \\ P^-_{|1;n\rangle}(u) &= P^-_{|0\rangle}(u)\, b(u - \nu_n)\, b(u + \nu_n) + P^+_{|0\rangle}(u)\, c(u - \nu_n)\, c(u + \nu_n). \end{aligned} \tag{26}$$

Note that $P^\pm_{|1;0\rangle}(u) = \overline{P^\mp_{|0\rangle}(u)}$, where $\overline{P^\pm(u)}$ is $P^\pm(u)$ under the transformation $\xi \to \pi(\lambda + 1) - \xi$. The reason for this is clear if we look back at figure 1; this transformation is equivalent to reflecting the diagram in the horizontal axis, interchanging the ground and first excited states.

Perhaps the neatest way to write the new reflection factors is

$$P^\pm_{|1;n\rangle}(u) = \overline{P^\mp(u)}\, a^1_n(u) \tag{27}$$

where

$$a^1_n(u) = \frac{a(u + \nu_n)\, a(u - \nu_n)}{a(u + \nu_0)\, a(u - \nu_0)}. \tag{28}$$

The factor $a^1_n(u)$ simplifies to

$$a^1_n(u) = \prod_{x=1}^{n} \frac{(\xi/\lambda\pi + 1/2\lambda - x/\lambda)\,(\xi/\lambda\pi - 1/2\lambda - x/\lambda)}{(\xi/\lambda\pi + 1/2\lambda - x/\lambda + 1)\,(\xi/\lambda\pi - 1/2\lambda - x/\lambda + 1)}. \tag{29}$$

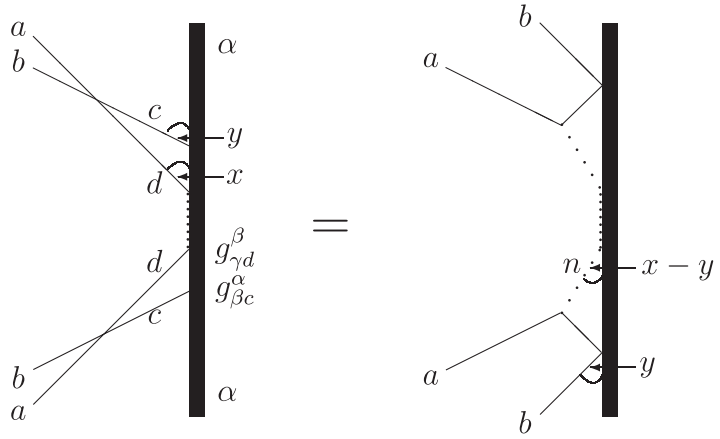

Figure 9. States can be created either by breathers or solitons.

Looking at the pole structure, we find that the functions $\overline{P^{\pm}(u)}$ have common simple poles at ν_0 and ν_{-N} where $N = 1, 2, 3, \ldots$. In addition, $\overline{P^{+}(u)}$ has simple poles at $u = w_{N'}$, where

$$w_{N'} = \pi - \frac{\xi}{\lambda} - \frac{\pi(2N'-1)}{2\lambda} = \overline{\nu_{N'}} \tag{30}$$

and $N' = 1, 2, 3, \ldots$, and simple zeros at $-w_{N''}$ for appropriate values of N''. Finally, $a_n^1(u)$ has simple poles at ν_0 and ν_n, and double poles at ν_k, $k = 1, 2, \ldots, n-1$.

Before proceeding to a more rigorous discussion, we shall now digress to give an outline of how the bootstrap might be expected to work. If one of these poles *does* correspond to a new bound state, factorizability leads us to expect that moving the soliton and antisoliton trajectories past each other (so that the antisoliton is incident on the boundary first) should also create the same state. The most obvious explanation for this would be for the antisoliton to bind to the boundary first, followed by the soliton, to form the state. From above, however, only solitons can bind to the ground state, so we must look further.

The *next* most obvious way this could happen is via the soliton and antisoliton forming a breather, either before or after the antisoliton has reflected from the boundary. The poles required to allow the first process (of the form $\pi + \frac{\xi}{\lambda} - \frac{\pi(2m+1)}{2\lambda}$) are not present, whereas those necessary for the second (of the form w_m) are. Our candidate process therefore becomes figure 9, where the soliton and antisoliton bind to form a breather, which then creates the state in one step. It is quite difficult to imagine any further alternatives, so let us (for the moment) take the existence of such a process as a necessary condition for a pole to be responsible for the formation of a boundary state.

The consequence of this is that the w_N poles are selected as the only possible candidates, and it appears that new bound states can only be formed by antisolitons. Such states hence have charge 0 (agreeing with the idea that they can also be formed from the ground state by the action of a breather). In addition, it is also clear that only those w_N such that $w_N < \nu_n$ can be considered, as, otherwise, the breather version of the process would see the breather created heading away from the boundary, rather than towards it.

Designating such a new state as $|0; n, N\rangle$ and bootstrapping on it leads to

$$\begin{aligned} P^{-}_{|0;n,N\rangle}(u) &= P^{-}_{|1;n\rangle}(u)\, a(u - w_N)\, a(u + w_N) \\ P^{+}_{|0;n,N\rangle}(u) &= P^{+}_{|1;n\rangle}(u)\, b(u - w_N)\, b(u + w_N) + P^{-}_{|1;n\rangle}(u)\, c(u - w_N)\, c(u + w_N). \end{aligned} \tag{31}$$

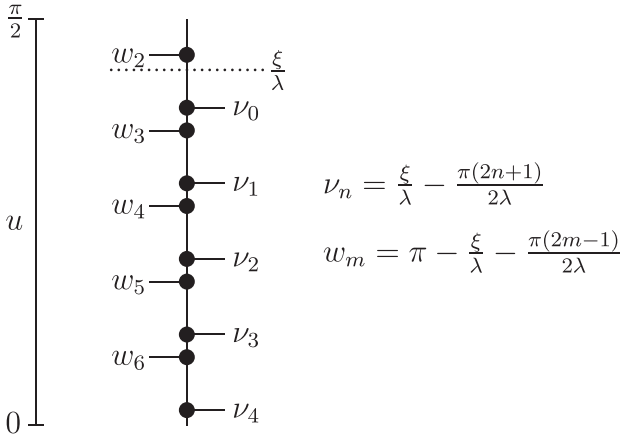

Figure 10. Location of poles. (Note that, in this case, w_2 can never participate in bound state formation as it is above ν_0.)

Substituting in (27) and taking advantage of the fact that $w_N = \overline{\nu_N}$ (so $a(u \pm w_N) = \overline{a(u \pm \nu_N)}$), this becomes

$$\begin{aligned} P^{-}_{|0;n,N\rangle}(u) &= a^1_n(u)\overline{P^{+}_{|0\rangle}(u)}\, a(u-\overline{\nu_N})\, a(u+\overline{\nu_N}) \\ P^{+}_{|0;n,N\rangle}(u) &= a^1_n(\overline{P^{-}_{|0\rangle}(u)}\, b(u-\overline{\nu_N})\, b(u+\overline{\nu_N}) + \overline{P^{+}_{|0\rangle}(u)}\, c(u-\overline{\nu_N})\, c(u+\overline{\nu_N})) \end{aligned} \tag{32}$$

which (apart from an extra factor of $a^1_n(u)$) is just the first bootstrap (26) under the transformation $\xi \to \pi(\lambda+1) - \xi$ and with solitons and antisolitons interchanged on the left-hand side. Thus, the pole structure follows naturally from the above. This can also be written as

$$P^{\pm}_{|0;n,N\rangle}(u) = P^{\pm}_{|0\rangle}(u)\, a^1_n(u)\, \overline{a^1_N(u)}. \tag{33}$$

Repeating the factorization argument shows that now we should focus on $\nu_{n'}$ poles such that $\nu_{n'} < w_N$. These are present now in the solitonic factor, though (due to the extra factor of $a^1_n(u)$) only for $n' > n$. However, since any such state obeys $\nu_n > w_N > \nu_{n'}$ in any case, this restriction is not relevant. The resultant state must now have charge 0.

A pattern is emerging, and it is not hard to see how the process would continue. Starting from the ground state, and taking the broadest guess (given our assumptions) for the spectrum, states can be formed by alternating solitons and antisolitons, the solitons having rapidity ν_{n_i} and the antisolitons having rapidity w_{N_j} (for some sets $\underline{n}$ and $\underline{N}$). An schematic pole structure is shown in figure 10, in terms of which the criterion for a state to be in the spectrum should be that we begin with one of the ν_n and then, as we move along the index list, move down the diagram, switching from side to side as we go. If we finish on a ν_m (indicating that the most recent particle to bind was a soliton) the state has charge 1 while, if we finish on a w_m (meaning an antisoliton) the state has charge 0.

Annotating such a state by its topological charge, c, and the sets $\underline{n}$ and $\underline{N}$ as $|c; n_1, N_1, n_2, N_2, \ldots\rangle$ (noting $\nu_{n_1} > w_{N_1} > \nu_{n_2} > w_{N_2} > \cdots$), the solitonic reflection factors should be

$$P^{\pm}_{|c;n_1,N_1,\ldots\rangle}(u) = P^{\pm}_{(c)}(u)\, a^1_{n_1}(u)\, \overline{a^1_{N_1}(u)} \ldots \tag{34}$$

with $P^{\pm}_0(u) = P^{\pm}_{|0\rangle}(u)$ and $P^{\pm}_1(u) = \overline{P^{\pm}_{|0\rangle}(u)}$. From now on, however, it will be more convenient to consider a single index list, and denote $\overline{a^1_m(u)}$ as $a^0_m(u)$, giving

$$P^{\pm}_{|c;n_1,n_2,\ldots,n_k\rangle}(u) = P^{\pm}_{(c)}(u)\, a^1_{n_1}(u)\, a^0_{n_2}(u)\, a^1_{n_3}(u) \ldots a^c_{n_k}(u) \tag{35}$$

where c is 1 if k is odd, and 0 if k is even. We will call this a level k boundary bound state. If we choose the ground state mass to be $m_s \sin^2\left(\frac{\xi-\pi/2}{2\lambda}\right)$, the mass of this state is

$$m_{n_1,n_2,\ldots} = m_s \sin^2\left(\frac{\xi-\pi/2}{2\lambda}\right) + \sum_{i\ \text{odd}} m_s \cos(\nu_{n_i}) + \sum_{j\ \text{even}} m_s \cos(w_{n_j}) \tag{36}$$

$$= m_s \sin^2\left(\frac{\xi-\pi/2}{2\lambda}\right) + \sum_{i\ \text{odd}} m_s \cos\left(\frac{\xi}{\lambda} - \frac{(2n_i+1)\pi}{2\lambda}\right) \tag{37}$$

$$- \sum_{j\ \text{even}} m_s \cos\left(\frac{\xi}{\lambda} + \frac{(2n_j-1)\pi}{2\lambda}\right).$$

This choice is convenient in that, as ξ passes π/β, the masses of the ground and first excited states interchange, in line with the idea that the states themselves swap at this point. An important point to note is that, in deriving all of this, we have simply been considering the soliton sector. However, we will see that allowing breather processes as well does not give rise to any further states, merely additional ways to jump between states. The Dirichlet boundary condition is also special in that either the soliton or the antisoliton can couple to a given boundary, but not both, as might be expected generically.

Although we have built up the states by applying the solitons and antisolitons in this alternating fashion, precisely how this happens in a given situation will of course depend on the impact parameters of the incoming particles. In figure 9 we already gave an example of the complicated way in which a process may be rearranged as these impact parameters vary, and the particular choices that we have adopted are mainly motivated by a desire to assemble the full spectrum in the simplest possible way.

4.3. Breather ground state reflection factors

We now return to the pole analysis, and examine the breather ground state reflection factors (17). Again, the factor R_0^n is boundary independent, and so all its poles should have an explanation in terms of the bulk. There are (physical strip) poles at $\frac{\pi}{2}$, $\frac{l\pi}{2\lambda}$, $\frac{\pi}{2} - \frac{n\pi}{2\lambda}$, and double poles at $\frac{\pi}{2} - \frac{l\pi}{2\lambda}$, with $l = 1, 2, \ldots, n-1$. There are no zeros. The pole at $\frac{\pi}{2}$ is simply due to the breather coupling perpendicularly to the boundary, while the poles at $\frac{l\pi}{2\lambda}$ are explained by figure 11. Next, the pole at $\frac{\pi}{2} - \frac{n\pi}{2\lambda}$ comes from a breather version of figure 7(a), B_{2n} being formed. Finally, the double poles at $\frac{\pi}{2} - \frac{l\pi}{2\lambda}$ are due to figure 12.

Moving on to the boundary-dependent part, there are poles at

$$u = \frac{\xi}{\lambda} - \frac{\pi}{2} \pm \frac{l\pi}{2\lambda} \tag{38}$$

and zeros at

$$u = -\frac{\xi}{\lambda} + \frac{\pi}{2} \pm \frac{l\pi}{2\lambda} \qquad u = \frac{\xi}{\lambda} + \frac{\pi}{2} \pm \frac{l\pi}{2\lambda} \tag{39}$$

where, for a breather n, $l = n-1, n-3, \ldots, l \geqslant 0$.

The set of poles can be rewritten by noting that, for breather m, there is a simple pole of the form $\frac{1}{2}(\nu_n - w_N)$ for all $n, N \geqslant 0$ and $n, N \in Z$ such that $m = n + N$. This ties in with the discussion in the previous section, since these are the rapidities predicted for the single-step process which is equivalent to a soliton binding at an angle of ν_n followed by an antisoliton at w_N.

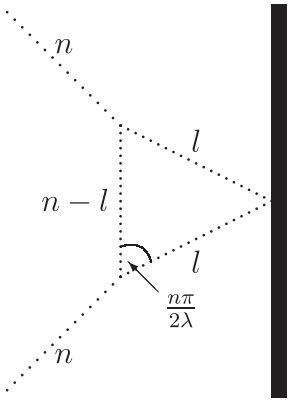

Figure 11. Process involving a breather triangle.

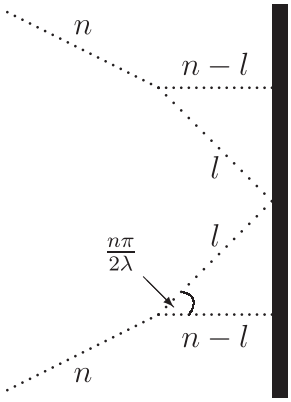

Figure 12. Process involving a double triangle of breathers.

4.4. Breather excited state reflection factors

Following the discussion of the solitonic excited state reflection factors, we can introduce corresponding breather reflection factors:

$$R^n_{|c;n_1,n_2,\ldots,n_k\rangle}(u) = R^n_{(c)}(u)\, a^{1;n}_{n_1}(u)\, a^{0;n}_{n_2}(u)\, a^{1}_{n_3}(u) \ldots a^{c;n}_{n_k}(u) \tag{40}$$

where $R^n_0(u) = R^n_{|0\rangle}(u)$ and $R^n_1(u) = \overline{R^n_{|0\rangle}(u)}$. We have also defined

$$a^{c;m}_n(u) = a^c_n\left(u + \frac{u_m}{2}\right) a^c_n\left(u - \frac{u_m}{2}\right) \tag{41}$$

or

$$a^{1;m}_n(u) = \prod_{x=1}^{m}\left[\frac{\left(\xi/\lambda\pi + (1-2x-n)/2\lambda + \frac{1}{2}\right)\left(\xi/\lambda\pi - (1+2x+n)/2\lambda + \frac{1}{2}\right)}{\left(\xi/\lambda\pi + (1-2x-n)/2\lambda - \frac{1}{2}\right)\left(\xi/\lambda\pi - (1+2x+n)/2\lambda - \frac{1}{2}\right)}\right.$$
$$\left.\times\,\frac{\left(\xi/\lambda\pi + (1-2x+n)/2\lambda - \frac{1}{2}\right)\left(\xi/\lambda\pi - (1+2x-n)/2\lambda - \frac{1}{2}\right)}{\left(\xi/\lambda\pi + (1-2x+n)/2\lambda + \frac{1}{2}\right)\left(\xi/\lambda\pi - (1+2x-n)/2\lambda + \frac{1}{2}\right)}\right] \tag{42}$$

with $a^{0;m}_n(u) = \overline{a^{1;m}_n(u)}$.

For $\overline{R^m_{|0\rangle}(u)}$, there are poles at

$$\begin{aligned} u &= \frac{\pi}{2} - \frac{\xi}{\lambda} + \frac{\pi}{\lambda} \pm \frac{l\pi}{2\lambda} \\ u &= \frac{\pi}{2} + \frac{\xi}{\lambda} - \frac{(l+2)\pi}{2\lambda} \end{aligned} \tag{43}$$

and zeros at

$$u = \frac{\xi}{\lambda} - \frac{\pi}{2} + \frac{(l-2)\pi}{2\lambda}. \tag{44}$$

For the other factors, $a_n^{1;m}(u)$ has physical strip poles/zeros at

$$\begin{aligned}
u &= -\frac{\xi}{\lambda} + \frac{\pi}{2} + \frac{p\pi}{2\lambda} && \text{poles:} \quad p = 2n - m + 2x \pm 1 \\
& && \text{zeros:} \quad p = -m + 2x \pm 1 \\
u &= \frac{\xi}{\lambda} - \frac{\pi}{2} + \frac{p\pi}{2\lambda} && \text{poles:} \quad p = m - 2x \pm 1 \\
& && \text{zeros:} \quad p = -2n + m - 2x \pm 1 \\
u &= \frac{\xi}{\lambda} + \frac{\pi}{2} + \frac{p\pi}{2\lambda} && \text{poles:} \quad p = -2n + m - 2x \pm 1 \\
& && \text{zeros:} \quad p = m - 2x \pm 1
\end{aligned} \tag{45}$$

while $a_n^{0;m}(u)$ has them at

$$\begin{aligned}
u &= -\frac{\xi}{\lambda} + \frac{3\pi}{2} + \frac{p\pi}{2\lambda} && \text{poles:} \quad p = -2N - m + 2x \pm 1 \\
& && \text{zeros:} \quad — \\
u &= -\frac{\xi}{\lambda} + \frac{\pi}{2} + \frac{p\pi}{2\lambda} && \text{poles:} \quad p = -m + 2x \pm 1 \\
& && \text{zeros:} \quad p = -2N - m + 2x \pm 1 \\
u &= \frac{\xi}{\lambda} - \frac{\pi}{2} + \frac{p\pi}{2\lambda} && \text{poles:} \quad p = 2N + m - 2x \pm 1 \\
& && \text{zeros:} \quad p = m - 2x \pm 1 \\
u &= \frac{\xi}{\lambda} + \frac{\pi}{2} + \frac{p\pi}{2\lambda} && \text{poles:} \quad p = m - 2x \pm 1 \\
& && \text{zeros:} \quad p = 2N + m - 2x \pm 1.
\end{aligned} \tag{46}$$

These poles will be further discussed in section 6 below.

5. An example

To gain an idea of the full picture, and which processes are responsible for the remaining poles, we will now look at one particular example in more detail. If we select $\xi = 1.6\pi$ and $\lambda = 2.5$, then we have the first two breathers in the spectrum, with the solitonic poles taking the form $\nu_n = \frac{\pi(2.2-2n)}{5}$ and $w_N = \frac{\pi(2.8-2N)}{5}$. Thus, for this case, only the poles at ν_0, ν_1 and w_1 are on the physical strip, and so figure 10 is simplified to figure 13. This is the simplest case which requires a broader spectrum than that postulated in [7]. First, let us turn to the soliton sector.

5.1. Boundary ground state: soliton sector

As argued above, the soliton can bind to the boundary at all rapidities ν_n which are in the physical strip, here just comprising ν_0 and ν_1. This introduces the states $|1; 0\rangle$ and $|1; 1\rangle$.

5.2. Boundary ground state: breather sector

The only breather poles are at $\frac{\xi}{\lambda} - \frac{\pi}{2} + \frac{(m-1)\pi}{2\lambda}$ for breather m. In addition, breather B_2 has a zero at $-\frac{\xi}{\lambda} + \frac{\pi}{2} + \frac{\pi}{2\lambda}$.

By lemma 1, the pole for B_1 must correspond to a new bound state, the rapidity being less than $\frac{\pi}{2\lambda}$. From figure 9, it is clear that B_1 creates the state which was labelled $|\delta_{0,1}\rangle$ in [7], and which we have called $|0; 0, 1\rangle$.

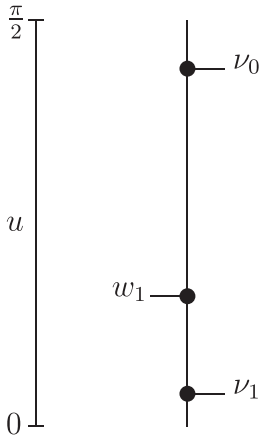

Figure 13. Location of poles in the example.

The pole for the second breather can be explained by figure B5, with the state $|1;0\rangle$ being formed. The antisoliton is reflected from the boundary at a rapidity of $\frac{\xi}{\lambda} - \pi + \frac{3\pi}{2\lambda}$—a zero of the $|1;0\rangle$ reflection factor—reducing the diagram to first order through the boundary Coleman–Thun mechanism.

5.3. First-level excited states: soliton sector

From before, $P^{+}_{|1;0\rangle}$ just has a simple pole at ν_0, which can be explained by the crossed process in figure 7(*c*), reducing the boundary to the ground state. For $P^{+}_{|1;1\rangle}$, the pole at ν_1 can be explained in this way, while, for the double pole at ν_0, figure B4 is required, the first breather being formed while the boundary is reduced to the vacuum state.

For $P^{-}_{|1;n\rangle}(u)$, we have the additional job of explaining simple poles at w_N, for all N such that this pole is in the physical strip. Here, this is only w_1. For $|1;0\rangle$, this is appropriate for the formation of $|0;0,1\rangle$ which, from the previous section, must be present. For $|1;1\rangle$, however, figure B3 is invoked, the second breather being created, and the boundary reduced to the vacuum state. The breather is incident on the boundary at an angle of $\frac{1}{2}(w_1 - \nu_1) = \pi - \frac{\xi}{\lambda} - \pi/2\lambda$ which, looking at the above breather reflection factors, is a zero, ensuring the diagram is of the correct order.

5.4. First-level excited states: breather sector

The pole structure of $R^{m}_{|1;0\rangle}$ can be found from $\overline{R^{m}_{|0\rangle}}$, and is

$$\begin{aligned} &B_1: \qquad \text{pole at} \quad \frac{\pi}{2} - \frac{\xi}{\lambda} + \frac{\pi}{\lambda} \\ &B_2: \qquad \text{poles at} \quad \frac{\pi}{2} - \frac{\xi}{\lambda} + \frac{3\pi}{2\lambda}, \frac{\pi}{2} - \frac{\xi}{\lambda} + \frac{\pi}{2\lambda}. \end{aligned} \tag{47}$$

By lemma 1, the second pole for B_2 must correspond to a new bound state; by the previous arguments, this is $|1;0,1,1\rangle$. This state is not in the spectrum given in [7], but lemma 1 shows that there is no way to avoid its introduction. Considerations such as this will open the door to a much wider spectrum in the general case.

The B_1 pole is suitable for the creation of $|1;1\rangle$. The first pole for B_2 can be explained by figure B7, with the boundary being reduced to the ground state by emission of a soliton.

For $R^m_{|1;1\rangle}$, the above poles are supplemented by additional poles from $b^1_{m,1}(u)$ to give the poles shown in table 1.

Table 1. Breather pole structure for $|1;1\rangle$. Entries are the values of p for which there is a pole in the location given in the column heading. The power of the entry gives the order of the pole, so e.g. 3^2 indicates a double pole when $p = 3$. There are no physical strip zeros for either breather.

	$-\frac{\xi}{\lambda}+\frac{\pi}{2}+\frac{p\pi}{2\lambda}$	$\frac{\xi}{\lambda}-\frac{\pi}{2}+\frac{p\pi}{2\lambda}$	$\frac{\xi}{\lambda}+\frac{\pi}{2}+\frac{p\pi}{2\lambda}$
B_1	2	0	—
B_2	3^2	1	-5

The pole at $\frac{\xi}{\lambda}+\frac{\pi}{2}-\frac{5\pi}{2\lambda}$ can be explained by figure B8, with the boundary being reduced to the ground state by emission of a soliton. The pole at $\frac{\xi}{\lambda}-\frac{\pi}{2}$ for B_1 can be allocated to the creation of $|1;0,1,1\rangle$, while the pole at $\frac{\xi}{\lambda}-\frac{\pi}{2}+\frac{\pi}{2\lambda}$ for B_2 is due to figure B9, where the boundary emits B_1, being reduced to $|1;0\rangle$.

The pole at $-\frac{\xi}{\lambda}+\frac{\pi}{2}+\frac{2\pi}{2\lambda}$ for B_1 is responsible for this reduction to $|1;0\rangle$, while the double pole for B_2 comes from an all-breather version of figure B6, the boundary being reduced in the same way.

5.5. Second-level excited states: soliton sector

For $P^-_{|0;0,1\rangle}(u)$, the only poles are simple, at ν_0 and w_1. The pole at w_1 can be explained by figure 7(c) while, for ν_0, we need figure B2. The second breather is emitted by the boundary, reducing it to the ground state, while a soliton is incident on the boundary at a rapidity w_1. For the ground state, this is neither a pole nor a zero, but the diagram contains a solitonic loop which can either be drawn to leave a soliton or an antisoliton incident on the boundary. Adding the contributions of these two diagrams gives an additional zero.

For $P^+_{|0;0,1\rangle}(u)$, we have additional poles at all ν, i.e. a simple pole at ν_1, with ν_0 becoming a double pole. By lemma 1, ν_1 must correspond to the creation of a new bound state, namely $|1;0,1,1\rangle$, while, for ν_0, figure B3 should be considered. Again, the second breather is created, the boundary is reduced to the ground state, and the breather is incident on the boundary at a rapidity of $\frac{1}{2}(\nu_0 - w_1) = \xi/\lambda - \pi/2$—a zero of the reflection factor.

5.6. Second-level excited states: breather sector

For $|0;0,1\rangle$, we have the pole structure given in table 2.

Table 2. Breather pole structure for $|0;0,1\rangle$.

	$-\frac{\xi}{\lambda}+\frac{3\pi}{2}+\frac{p\pi}{2\lambda}$	$-\frac{\xi}{\lambda}+\frac{\pi}{2}+\frac{p\pi}{2\lambda}$	$\frac{\xi}{\lambda}-\frac{\pi}{2}+\frac{p\pi}{2\lambda}$
B_1	-2	2	0, 2
B_2	-3	3	1^2

The poles at $-\frac{\xi}{\lambda}+\frac{3\pi}{2}+\frac{p\pi}{2\lambda}$ are due to figure B8, while the poles in the second column are due to figure B9. For all these, the boundary is reduced to $|1;0\rangle$. The pole at $\frac{\xi}{\lambda}-\frac{\pi}{2}+\frac{(m-1)\pi}{2\lambda}$ for B_m ($m = 2$) is due to figure B12, while for $m = 1$ it is due to a breather version of figure 7(c). The pole at $\frac{\xi}{\lambda}-\frac{\pi}{2}+\frac{2\pi}{2\lambda}$ for B_1 is due to figure B7.

5.7. Third-level excited states: soliton sector

The only third-level excited state is $|1; 0, 1, 1\rangle$. For $P^{+}_{|1;0,1,1\rangle}$, there are simple poles at w_1, ν_0 and ν_1. Again, the pole at w_1 comes from the crossed process figure 7(c). For ν_1, figure 7(c) suffices while, for ν_0, figure B4 is required, the boundary being reduced to $|0; 0, 1\rangle$, while the first breather is incident on the boundary at $\frac{\pi}{2} - \frac{\xi}{\lambda} + \frac{\pi}{\lambda}$, another zero.

5.8. Third-level excited states: breather sector

Here, we find the poles given in table 3.

Table 3. Breather pole structure for $|1; 0, 1, 1\rangle$.

	$-\frac{\xi}{\lambda} + \frac{3\pi}{2} + \frac{p\pi}{2\lambda}$	$-\frac{\xi}{\lambda} + \frac{\pi}{2} + \frac{p\pi}{2\lambda}$	$\frac{\xi}{\lambda} - \frac{\pi}{2} + \frac{p\pi}{2\lambda}$	$\frac{\xi}{\lambda} + \frac{\pi}{2} + \frac{p\pi}{2\lambda}$
B_1	-2	$2^2, 4$	$0, 2$	—
B_2	-3	$1, 3^3$	1^2	-5

Comparing this with the structure given above for $|1; 1\rangle$, it can easily be seen that, whenever the two both have a pole at the same rapidity, essentially the same explanation can be used. For the remaining poles, $-\frac{\xi}{\lambda} + \frac{3\pi}{2} + \frac{p\pi}{2\lambda}$ can be explained by figure B9, the boundary being reduced to $|1; 0\rangle$, while that at $-\frac{\xi}{\lambda} + \frac{\pi}{2} + \pi/2\lambda$ for B_2 is due to figure 7(c), reducing the boundary to $|1; 0\rangle$, and that at $\frac{\xi}{\lambda} - \frac{\pi}{2} + \frac{2\pi}{2\lambda}$ for B_1 is due to an all-breather version of figure B7, again reducing the boundary to $|1; 0\rangle$.

5.9. Summary

The above has shown that, by introducing only the states which are required by lemmas 1 and 2, the complete pole structure can be explained. Below, we shall find that this is a general feature. In addition, the spectrum of states is broader than that introduced in [7] (containing, in addition to their states, $|1; 0, 1, 1\rangle$). It should be noted that the mass of this extra state corresponds to $m_{1,1}$ of [7], the mass of a boundary Bethe ansatz (1, 1)-string whose apparent absence from the bootstrap spectrum was described in that paper as 'confusing'. This does at least show that the Bethe ansatz results of [7] are not incompatible with the bootstrap. However, in more general cases it turns out that the bootstrap predicts yet further states, beyond those identified in the boundary Bethe ansatz calculations of [7], so a full reconciliation of the Bethe ansatz and bootstrap approaches remains an open problem.

6. The general case

From the above, we might be tempted to guess that the boundary state labelled by $|c; n_1, n_2, n_3, \ldots, n_m\rangle$ exists iff c is 0 or 1 and $n_1, n_2, n_3, \ldots$ are chosen such that $\pi/2 > \nu_{n_1} > w_{n_2} > \nu_{n_3} > \cdots > 0$. This turns out to be correct, and will be proved in two stages. Firstly, we need to show that all of these states must be present, before going on to show that, given this, all other poles can be explained without invoking further boundary states.

6.1. The minimal spectrum

The argument proceeds as follows: starting with the knowledge that the vacuum state $|0\rangle$ and all appropriate states $|1; n_1\rangle$ are in the spectrum, we use breather poles to construct all the other postulated states.

These poles are of the form $\frac{1}{2}(w_N - v_n)$ for breather $n+N$ incident on a charge 0 state (or $\frac{1}{2}(v_n - w_N)$ for a charge 1 state). If $v_n - w_N < \frac{\pi}{\lambda}$, lemma 1 shows that they must correspond either to the formation of a new state, or the crossed process. From figure 9, this corresponds either to adding indices n and N if they are absent or—if they are already present—removing them. (Note that any other option would give rise to a state with a mass outside the scheme given by (38), and therefore outside our postulated spectrum.) The condition $v_n - w_N < \frac{\pi}{\lambda}$ is always satisfied if $v_n > w_N$ and v_n and w_N are as close together as possible, i.e. if $|0; n, N\rangle$ exists, but $|0; n, N-1\rangle$ does not.

The only subtlety in this argument arises when considering the topmost breather. If $n+N = n_{\max}$, lemma 1 on its own is not strong enough to require the presence of the state we need, and we must invoke the stronger version introduced at the end of section 3. This makes use the idea that there must be a corresponding two-stage solitonic route to the same state, i.e. a soliton with rapidity v_n followed by an antisoliton with rapidity w_N. Considering these two processes instead, the stronger lemma shows that both form bound states, as v_n and w_N must be the lowest poles of their type—and so have a rapidity of less than $\frac{\pi}{\lambda}$—for $n+N$ to equal $n_{\max}$. This shows that the state exists, and hence that the breather pole is due to its formation.

Since the arguments for the two sectors are analogous, let us focus on the charge 0 sector here. The challenge is to create any state $|0; \underline{x}\rangle$ (for some set of indices $\underline{x} = (n_1, n_2, \ldots, n_{2k})$) from the ground state using just these poles. As a first step, consider creating $|0; n_1, n_2\rangle$. If v_{n_1} and w_{n_2} are as close together as possible, we simply make use of the pole at $\frac{1}{2}(w_{n_2} - v_{n_1})$. Otherwise, introduce the set $m_1, m_2, \ldots, m_t$ such that $v_{n_1} > w_{m_1} > v_{m_2} > w_{m_3} > \cdots > v_{m_t} > w_{n_2}$, with each successive rapidity as close to the previous one as possible. Now, we can successively create $|0; \underline{x}, n_1, m_1\rangle$, then $|0; \underline{x}, n_1, m_1, m_2, m_3\rangle$ and so on, up to $|0; \underline{x}, n_1, m_1, m_2, m_3, \ldots, m_t, n_2\rangle$.

By now invoking the crossed process, a suitable breather can be used to remove the indices m_1, m_2, followed by m_3, m_4 and so on, until all the m indices have been removed to leave $|0; \underline{x}, n_1, n_2\rangle$.

Repeating this procedure allows $|0; n_1, n_2, n_3, n_4\rangle$ to be created, and hence $|0; \underline{x}\rangle$. Note that this allows any state in our allowed spectrum to be created, but no others, as the condition $v_{n_1} > w_{n_2} > \cdots$ is imposed by the existence of the necessary breather poles. Charge 1 states can be created analogously by starting from a suitable state $|1; n_1\rangle$.

One remaining point is to check that all the necessary breather poles do indeed exist. However, starting from (40), they occur in the $R^n_{(c)}(u)$ factor, and it is straightforward to check that they are never modified by the other a factors.

6.2. Reflection factors for the minimal spectrum

The boundary state can be changed by the solitonic processes given in table 4.

Table 4. Solitonic processes which change the boundary state.

Initial state	Particle	Rapidity	Final state
$\|0; n_1, \ldots, n_{2k}\rangle$	Soliton	v_n	$\|1; n_1, \ldots, n_{2k}, n\rangle$
$\|1; n_1, \ldots, n_{2k-1}\rangle$	Antisoliton	w_N	$\|0; n_1, \ldots, n_{2k-1}, N\rangle$

The breather sector is more complex, as indices can be added or removed from any point in the list, and not just at the end, as for solitons. In addition, processes exist which simply adjust the value of one of the indices, rather than increasing the number of indices. For breather m,

Table 5. Breather processes which change the boundary state.

Initial state	Rapidity	Final state
$\|0/1; \ldots n_{2x}, n_{2x+1} \ldots\rangle$	$\frac{1}{2}(v_n - w_N), n+N=m$	$\|0/1; \ldots n_{2x}, n, N, n_{2x+1} \ldots\rangle$
$\|0/1; \ldots n_{2x-1}, n_{2x} \ldots\rangle$	$\frac{1}{2}(w_N - v_n), n+N=m$	$\|0/1; \ldots n_{2x-1}, N, n, n_{2x} \ldots\rangle$
$\|0/1; \ldots n_{2x} \ldots\rangle$	$\frac{1}{2}(v_{-n_{2x}} - w_{n_{2x}+m})$	$\|0/1; \ldots n_{2x}+m \ldots\rangle$
$\|0/1; \ldots n_{2x-1} \ldots\rangle$	$\frac{1}{2}(w_{-n2x-1} - w_{n_{2x-1}+m})$	$\|0/1; \ldots n_{2x-1}+m \ldots\rangle$

these are given in table 5. This should be read as implying that any index can have its value raised, and that a pair of indices can be inserted at any point in the list, including before the first index and after the last (providing the resultant state is allowed). Both of these tables have been derived on the basis that, whenever assuming that a pole corresponds to a bound state leads to a state with the same mass and topological charge as one in our minimal spectrum, the assumption is taken to be correct. As with our earlier assumption (that, if a pole has another possible explanation, it is not taken as forming a bound state), this is intuitively reasonable but not necessarily rigorous. It does, however, lead to consistent results, and there is no conflict between the two assumptions: we have been unable to find any alternative explanation for any of the poles listed above.

It is vital for what follows that, for all the above processes, there is very little dependence on the existing boundary state. For the solitons, the topological charge of the state and the value of the last index in the list are all that matter. Any two states which have the same topological charge and last index can undergo processes at the same rapidities to add an index. Similarly, for the breathers, provided either the relevant two indices can be added at some point in the list to create an allowed state, or that the index to be adjusted is present in the list, the other characteristics of the state are irrelevant.

6.3. Solitonic pole structure

This turns out to be relatively straightforward. All poles are either of the form v_n or w_N. Looking at a charge 0 state with $2k$ indices, and labelling this as $|0;\underline{x}\rangle = |0; n_1, n_2, \ldots, n_{2k}\rangle$, we find the results shown in table 6 for $P^-_{|0;\underline{x}\rangle}(u)$.

Table 6. Pole structure for $P^-_{|0;\underline{x}\rangle}(u)$. An entry of, for example, $w_1 \ldots w_{n_2-1}$ indicates that there is a pole of order $2k$ at $w_1, w_2, w_3, \ldots, w_{n_2-1}$.

Pole	Order	Pole
$w_1 \ldots w_{n_2-1}$	$2k$	$v_1 \ldots v_{n_1-1}$
w_{n_2}	$2k-1$	v_{n_1}
$w_{n_2+1} \ldots w_{n_4-1}$	$2k-2$	$v_{n_1+1} \ldots v_{n_3-1}$
w_{n_4}	$2k-3$	v_{n_3}
$\vdots$	$\vdots$	$\vdots$
$w_{n_{2k-2}+1} \ldots w_{n_{2k}-1}$	2	$v_{n_{2k-3}+1} \ldots v_{n_{2k-1}-1}$
$w_{n_{2k}}$	1	$v_{n_{2k-1}}$

These poles come from the a factors so, for P^+, there is an additional pole at all v. For the charge 1 states, the picture is very similar, and, considering P^+ first, we find the pattern given in table 7 for a state with $2k-1$ indices. In addition, there are poles at all w for P^-.

Table 7. Pole structure for $P^{+}_{|1;\underline{x})}(u)$.

Pole	Order	Pole
—	1	$\nu_0, \nu_{-1}, \ldots$
—	$2k$	$\nu_1 \ldots \nu_{n_1-1}$
—	$2k-1$	ν_{n_1}
$w_1 \ldots w_{n_2-1}$	$2k-2$	$\nu_{n_1+1} \ldots \nu_{n_3-1}$
w_{n_2}	$2k-3$	ν_{n_3}
$\vdots$	$\vdots$	$\vdots$
$w_{n_{2k-4}+1} \ldots w_{n_{2k-2}-1}$	2	$\nu_{n_{2k-3}+1} \ldots \nu_{n_{2k-1}-1}$
$w_{n_{2k-2}}$	1	$\nu_{n_{2k-1}}$

(For the charge 0 case, there are poles at w_x for $x \leqslant 0$, but none of these are in the physical strip.)

An important point to note is that, comparing the general level $2k$ state $|0; n_1, n_2, \ldots, n_{2k-1}, n_{2k}\rangle$ with the level 2 state $|0; n_{2k-1}, n_{2k}\rangle$, we find no additional poles, though the order of some poles has increased. In the example above, all level 2 states were explained by diagrams where the boundary was reduced either to the vacuum by emission of a breather, or to a first-level excited state by emission of an antisoliton. The same processes turn out to be present for any level $2k$ state to be reduced to a level $2k-1$ or $2k-2$ state. Thus, we might imagine explaining the poles in the level $2k$ reflection factor via similar processes to those which explained them in the level 2 factor. At times, however—as we shall see—parts of these processes will need to be replaced by more complex subdiagrams to allow for the fact that the boundary is in a higher excited state, explaining the differences in the orders of the poles. Considering the level 2 processes so far introduced as 'building blocks', this can be considered as an iterative process: level 4 states can be explained by replacing parts of level 2 processes with building blocks, while level 6 states can be explained by similarly replacing parts of level 4 processes with building blocks, and so on. A generic process of the type we will examine can therefore be viewed as a cascade of building blocks, each appearing as a subdiagram of the one before it.

A similar argument applies to level $2k+1$ states and level 3 states, drawing the same diagrams with all rapidities transformed via $\xi \to \pi(\lambda+1) - \xi$. We will concentrate on the charge 0 sector below, and consider a generic level $2k$ state.

For poles of the form ν_n, consider figure B13. The boundary decays to the state $|0; n_1, n_2, \ldots, n_{2k-2}\rangle$ by emission of breather $n_{2k}+n_{2k-1}$ at a rapidity of $\frac{1}{2}(\nu_{n_{2k-1}} - w_{n_{2k}})$. This then decays into breather $n_{2k-1}-n$ heading towards the boundary at a rapidity of $\frac{1}{2}(w_{-n_{2k-1}} - \nu_n)$ and breather $n_{2k}+n$ heading away from the boundary at a rapidity of $\nu_n - \left(\frac{\pi}{2} - \frac{(n_{2k}+n)\pi}{2\lambda}\right)$. This then decays to give the outgoing particle and one heading towards the boundary at a rapidity of $w_{n_{2k}}$. For $n < n_{2k-1}$, it is straightforward to check that all these rapidities are within suitable bounds.

This diagram is naively third order. However, breather $n_{2k-1}-n$, which is drawn as simply reflecting off the boundary, in fact has a pole, meaning that the diagram should be treated as schematic and the appropriate diagram from the next section inserted instead. In addition, as noted in the discussion of the example, the soliton loop contributes a zero for an incoming antisoliton through the Coleman–Thun mechanism. When this is taken into account, we obtain the correct result.

For ν_{2k-1}, the slightly simpler figure B2 suffices. The remaining ν poles are only present in the soliton reflection factor, and can be explained by figure B3, with the boundary decaying by

emitting an antisoliton at $w_{n_{2k}}$, which then interacts with the incoming soliton to give breather $n+n_{2k}$, heading towards the boundary at a rapidity of $\frac{1}{2}(\nu_n - w_{n_{2k}})$. Looking ahead again, the interaction of this breather with the boundary contributes the required zero. For $\nu_n < w_{n_{2k}}$, this diagram fails, the breather being created heading away from the boundary; this is the point when the pole is to be considered as creating the bound state $|1; n_1, \ldots, n_{2k}, n\rangle$.

For the w_N poles, the story is very similar, this time being based on figure B4 (requiring a suitable pole/zero for $B_{N-n_{2k}}$ on state $|1; n_1, \ldots, n_{2k-1}\rangle$ at $\frac{\xi}{\lambda} - \frac{\pi}{2} + \frac{\pi(N+n_{2k}-1)}{2\lambda}$) for $N < n_{2k}$ and figure 7(c) for n_{2k}. As noted above, all charge 1 state poles can be explained by the same mechanisms, with the rapidities transformed according to $\xi \to \pi(\lambda+1) - \xi$.

6.4. Breather pole structure

This is considerably more complicated. However, with a bit of work it turns out that, for breather n on the state $|0; n_1, n_2, \ldots, n_{2k}\rangle$, the pole structure is as given in table 8.

Table 8. Breather pole structure for a generic charge 0 state. The variable x takes integer and half-integer values within the allowed ranges. An entry in the third column represents a pole of that order if it is positive, and a zero of appropriate order if it is negative. (Thus an entry of +1 is a first-order pole, and an entry of −1 is a first-order zero.) Also, for convenience, y is 1 if x (or $|x|$) attains the lower limit, −1 if $n+x$ (or $n-|x|$) attains the lower limit, and zero otherwise, while i is 1 if x is integer, and 0 otherwise.

Pole	Range	Pole/zero order
$\frac{\xi}{\lambda} - \frac{\pi}{2} + \frac{\pi(n+2x-1)}{2\lambda}$	$n_{2q} < x < n_{2q+2}$ $n_{2q'} < n+x < n_{2q'+2}$	$2(q'-q)+y$
	$x < 0, n_{2q-1} < \lvert x\rvert < n_{2q+1}$ $n_{2q'} < n-\lvert x\rvert < n_{2q'+2}$	$2(q'-q)+y+i$
$-\frac{\xi}{\lambda} + \frac{\pi}{2} + \frac{\pi(n+2x+1)}{2\lambda}$	$n_{2q-1} < x < n_{2q+1}$ $n_{2q'-1} < n+x < n_{2q'+1}$	$2(q'-q)+y$
	$x < 0, n_{2q} < \lvert x\rvert < n_{2q+2},$ $n_{2q'-1} < n-\lvert x\rvert < n_{2q'+1}$	$2(q'-q)-i+y$
	$x < -n, n_{2q} < \lvert x\rvert < n_{2q+2}$ $n_{2q'} < \lvert x\rvert - n < n_{2q'+2}$	$2(q'-q)$
$\frac{\xi}{\lambda} + \frac{\pi}{2} + \frac{\pi(n+2x-1)}{2\lambda}$	As $\frac{\xi}{\lambda} - \frac{\pi}{2} + \frac{\pi(n+2x+1)}{2\lambda}$ with poles ↔ zeros	
$-\frac{\xi}{\lambda} + \frac{3\pi}{2} + \frac{\pi(n+2x+1)}{2\lambda}$	As $-\frac{\xi}{\lambda} + \frac{\pi}{2} + \frac{\pi(n+2x-1)}{2\lambda}$ with poles ↔ zeros	

In explaining all this, we can begin with the diagrams found previously. For the first line, consider an all-breather version of figure B5, where the breather decay is chosen to produce breather $n+x-n_{2q'}$ on the left, which then binds to the boundary to raise index $n_{2q'}$ to $n+x$. In some cases, this is not possible, the appropriate state not being in the spectrum, but, then, we can consider an all-breather version of figure B10, where the boundary decays so as to remove the indices $n_{2q'}$ and $n_{2q'+1}$, with the same initial breather decay, and the additional breather reflecting from the boundary contributes a zero. This diagram becomes possible just as the other fails. In either case, the other breather from the initial decay (which is drawn as simply reflecting from the boundary), is breather $y = n_{2q'} - x$ at rapidity $\frac{\xi}{\lambda} - \frac{\pi}{2} + \frac{\pi(y+2x-1)}{2\lambda}$. This has a pole of order two less than the initial breather. If this order is less than or equal to zero, the diagram stands as drawn while, otherwise, the simple reflection from the boundary should be

replaced by a repeat of this argument, iterating until the result is less than or equal to zero. For the next line, precisely the same argument can be used.

The next three lines can be explained by a similar argument, based on either increasing the value of the index $n_{2q'-1}$ or removing indices $n_{2q'-1}$ and $n_{2q'}$.

For $\frac{\xi}{\lambda} + \frac{\pi}{2} + \frac{\pi(n+2x-1)}{2\lambda}$, we invoke a similar process. This time, however, the outer legs have rapidity $v_{-(n+x)}$ (where $-(n+x)$ is actually a positive number if the initial pole is to be in the physical strip), and so we need to substitute in the explanation of soliton poles of this form from before, leading, in simple cases, to figure B9.

Finally, for $\frac{3\pi}{2} - \frac{\xi}{\lambda} + \frac{\pi(n+2x+1)}{2\lambda}$, we begin with figure B8. This time, the reflection factor for the central soliton always provides a zero, while the outer soliton has rapidity w_{n+x}. If $n + x = n_{2k}$, the diagram is as drawn while, otherwise, we need to replace the two outer antisoliton legs with the explanation of the appropriate pole in the antisoliton factor. The first iteration of this is shown in figure B10.

7. Conclusions

We now summarize our results. We have found that the spectrum of boundary bound states of the sine–Gordon model with Dirichlet boundary conditions can be characterized in terms of two 'sectors', having topological charges $\frac{\beta\varphi_0}{2\pi}$ and $1 - \frac{\beta\varphi_0}{2\pi}$ (which we labelled as '0' and '1', respectively). A boundary state can be described in an index notation as $|c; n_1, n_2, \ldots, n_k\rangle$ for topological charge c, with $c = 0$ for k even and $c = 1$ for k odd. Such a state can be created by a succession of alternating solitons and antisolitons, beginning with a soliton. The necessary soliton rapidities are of the form,

$$v_n = \frac{\xi}{\lambda} - \frac{\pi(2n+1)}{2\lambda} \tag{48}$$

while those for the antisolitons are

$$w_m = \pi - \frac{\xi}{\lambda} - \frac{\pi(2m-1)}{2\lambda}. \tag{49}$$

These are interchanged by the transform $\xi \to \pi(\lambda + 1) - \xi$. Any such state can be formed, provided the rapidities involved are monotonically decreasing, i.e. $v_{n_1} > w_{n_2} > v_{n_3} > \cdots$, and its mass is given by

$$m_{n_1,n_2,\ldots} = m_s \sin^2\left(\frac{\xi - \pi/2}{2\lambda}\right) + \sum_{i \text{ odd}} m_s \cos(v_{n_i}) + \sum_{j \text{ even}} m_s \cos(w_{n_j}) \tag{50}$$

$$= m_s \sin^2\left(\frac{\xi - \pi/2}{2\lambda}\right) + \sum_{i \text{ odd}} m_s \cos\left(\frac{\xi}{\lambda} - \frac{(2n_i+1)\pi}{2\lambda}\right)$$

$$- \sum_{j \text{ even}} m_s \cos\left(\frac{\xi}{\lambda} + \frac{(2n_j-1)\pi}{2\lambda}\right). \tag{51}$$

This spectrum is considerably larger than that suggested in [7], though all the states introduced are required to satisfy our lemmas. It is worth pointing out that a second part of the analysis of [7] involved an examination of the (boundary) Bethe ansatz for a lattice regularization of the model. Some of the masses which emerged in the course of that study—those of the (n, N)-strings—were outside the spectrum proposed in [7], but are now included as the masses of the states $|1; 0, n, N\rangle$. It remains to be seen, however, whether the other masses in our spectrum can be recovered in the Bethe ansatz approach.

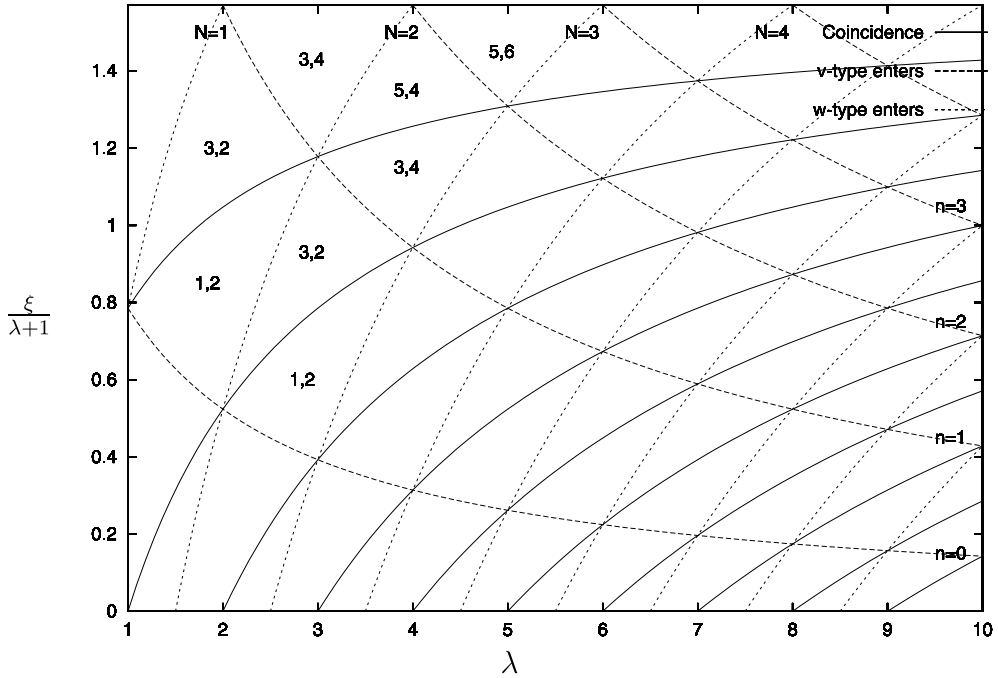

Figure 14. Boundary bound state spectrum size. The number of states present increases as v-type and w-type poles enter the physical strip, but changes also occur as the two sets of poles pass through coincidence: moving in the direction of increasing λ, the topmost relevant w-type pole passes v_0 and ceases to be relevant, reducing the spectrum. (Notation x, y implies $F(x)$ charge 0 states and $F(y)$ charge 1 states.)

The number of states present in the spectrum clearly depends on the boundary parameters, as illustrated in figure 14. It is convenient to express these in terms of Fibonacci numbers, $F(x)$, where $F(x) = 1, 1, 2, 3, 5, \ldots$ for $x = 0, 1, 2, \ldots$. If there are n v-type poles, and m relevant† w-type poles, there are, in general, $F(2n)$ charge 1 states and $F(2m + 1)$ charge 0 states. Explicitly, these are given by

$$\begin{aligned} n &= \left[\frac{\xi}{\pi} - \frac{1}{2}\right] + 1 \\ m &= \left[\frac{\lambda}{2} - \frac{\xi}{\pi} + \frac{1}{2}\right] - \left[\lambda - \frac{\xi}{\pi} + \frac{1}{2}\right] \end{aligned} \tag{52}$$

where the square brackets denote the integer part of the number. This changes when the two sets of poles coincide, in which case there are 2^{n-1} states in each sector.

Finally, we note that the general method used to derive the spectrum, via the simple geometrical argument leading to the two lemmas given in section 3, which can be applied equally well to any two-dimensional model. Using this to deduce the existence of as many states as possible led—in our case—to the full spectrum. In other cases, we may not be so fortunate, but, using it as a starting point, it should make the derivation of the full spectrum a finite (though possibly lengthy) task.

† A w-type pole with a rapidity greater than v_0 can never be involved in forming a bound state, and so is not 'relevant' here.

Acknowledgments

We are grateful to Aldo Delfino, Subir Ghoshal, Brett Gibson and Matthias Pillin for help and interesting discussions. We would especially like to thank Gustav Delius for his comments on a first draft of this paper. PM and PED thank the EPSRC for a Research Studentship and an Advanced Fellowship, respectively, and PED thanks SPhT Saclay and the Departamento de Física de Partículas, USC (Santiago de Compostela), for hospitality. The work was supported in part by a TMR grant of the European Commission, reference ERBFMRXCT960012.

Appendix A. Infinite products of gamma functions

The products which arise in the course of this work are of the form

$$P(u) = \prod_{l=1}^{\infty} \left[\frac{\Gamma(kl + a - xu)\Gamma(kl + b - xu)}{\Gamma(kl + c - xu)\Gamma(kl + d - xu)} \Big/ (u \to -u) \right] \tag{A1}$$

Rather than examine this product directly, we take logs and use the standard formula

$$\ln \Gamma(z) = z \ln(z) - z - \frac{1}{2} \ln(z) + \ln(\sqrt{2}) + \frac{1}{12z} + \mathrm{O}(z^{-3}). \tag{A2}$$

Assuming that the sum over l and the expansion in z can be exchanged, potential divergences arise from terms of the form $\sum_{l=1}^{\infty} \frac{a}{l^n}$ with $a \neq 0$ and $n < 2$. To begin with, we will consider the terms arising from the block of four terms explicitly shown.

Firstly, there is a contribution of $\sum_{l=1}^{\infty} a + b - c - d$ from the z terms, which can be set to zero by demanding $a + b = c + d$. For the $1/12z$ terms, the overall contribution from the four terms is

$$\sum_{l=1}^{\infty} \frac{1}{12} \left(\frac{a - c}{(kl + a - xu)(kl + c - xu)} + \frac{b - d}{(kl + b - xu)(kl + d - xu)} \right) \tag{A3}$$

which can be seen, for $a + b = c + d$, to be of the form $1/l^2$ and hence convergent.

A similar argument applies to the $-\frac{1}{2} \ln(z)$ terms, showing they also provide a convergent contribution. This breaks down when considering the $z \ln(z)$ terms, however, and their contribution formally reduces to

$$\sum_{l=1}^{\infty} \Big(\frac{cd - ab}{kl} + \mathrm{O}(l^{-2}) \Big) \tag{A4}$$

which is divergent unless $a = c$ or $b = c$, both of which are trivial cases. However, repeating this argument on the other block (with $u \to -u$) can be seen to yield the same result, allowing the two divergent terms to cancel, and leaving a product which is convergent overall.

For comparison with other results, it is useful to write $P(u)$ in other ways. Firstly, it can be written in terms of Barnes' diperiodic sine functions using the expansion as given in [11]:

$$\begin{aligned} S_2(x|\omega_1, \omega_2) = {} & \exp\left[\frac{(\omega_1 + \omega_2 - 2x)\,(\gamma + \log(2\pi) + 2\log(\omega_1/\omega_2))}{2\omega_1} \right] \frac{\Gamma\left((\omega_1 + \omega_2 - x)/\omega_1\right)}{\Gamma\left(x/\omega_1\right)} \\ & \times \prod_{n=1}^{\infty} \left[\frac{\Gamma\left((\omega_1 + \omega_2 - x + n\omega_2)/\omega_1\right)}{\Gamma\left((x + n\omega_2)/\omega_1\right)} \right. \\ & \left. \times \exp\left[-\frac{\omega_1 + \omega_2 - 2x}{2n\omega_1} \right] \left(\frac{n\omega_1}{\omega_2} \right)^{-(\omega_1 + \omega_2 - 2x)/\omega_1} \right] \end{aligned} \tag{A5}$$

where γ denotes the Euler constant. For blocks of the form we are interested in, this simplifies to

$$\frac{S_2(x_1|\omega_1,\omega_2)S_2(x_2|\omega_1,\omega_2)}{S_2(x_3|\omega_1,\omega_2)S_2(x_4|\omega_1,\omega_2)}$$

$$= \prod_{n=1}^{\infty}\left[\left\{\frac{\Gamma\left((\omega_1+n\omega_2)/\omega_1 - x_1/\omega_1\right)}{\Gamma\left((n-1)\omega_2/\omega_1 + x_1/\omega_1\right)}\frac{\Gamma\left((\omega_1+n\omega_2)/\omega_1 - x_2/\omega_1\right)}{\Gamma\left((n-1)\omega_2/\omega_1 + x_2/\omega_1\right)}\right\}\right.$$

$$\left./(x_{1,2}\to x_{3,4})\right] \tag{A6}$$

provided $x_1 + x_2 = x_3 + x_4$. Comparing with (A1) we have

$$P(u) = \frac{S_2(\omega_1(1-a+xu)|\omega_1,\omega_1 k)S_2(\omega_1(1-b+xu)|\omega_1,\omega_1 k)}{S_2(\omega_1(1-c+xu)|\omega_1,\omega_1 k)S_2(\omega_1(1-d+xu)|\omega_1,\omega_1 k)} \tag{A7}$$

where w_1 is arbitrary. In section 2 we took $\omega_1 = x^{-1}$ for simplicity. The identity

$$S_2(\omega_1+\omega_2-x|\omega_1,\omega_2) = \frac{1}{S_2(x|\omega_1,\omega_2)} \tag{A8}$$

was also used.

These products can also be written in an integral form, through

$$\log\Gamma(\zeta) = \int_0^{\infty}\frac{\mathrm{d}x}{x}\,\mathrm{e}^{-x}\left[\zeta - 1 + \frac{\mathrm{e}^{-(\zeta-1)x}-1}{1-\mathrm{e}^{-x}}\right] \mathrm{Re}\,\zeta > 0. \tag{A9}$$

Since, for the expressions we consider, not all the Γ-functions have arguments with a positive real part, it is not possible to give a general formula for P solely in these terms. Instead, we give expressions for the reflection factors. To simplify matters, define

$$I^1(u) = \frac{2\lambda}{\pi}\int_{-\infty}^{+\infty}\mathrm{d}x\,\cosh\left(\frac{2\lambda u x}{\pi}\right)\left[\frac{\sinh\left(\lambda - 2\xi/\pi\right)x}{2\sinh x\cosh\lambda x}\right] \tag{A10}$$

$$I^2(u) = \frac{2\lambda}{\pi}\int_{-\infty}^{+\infty}\mathrm{d}x\,\cosh\left(\frac{2\lambda u x}{\pi}\right)\left[\frac{\sinh\left(2\xi/\pi - 2n_* - 2\right)x}{\sinh x}\right] \tag{A11}$$

$$I_n^3(u) = -\frac{2\lambda}{\pi}\int_{-\infty}^{+\infty}\mathrm{d}x\,\cosh\left(\frac{2\lambda u x}{\pi}\right)\left[\frac{2\cosh x\sinh\left(\lambda+1+2n-2\xi/\pi\right)x}{2\sinh x\cosh\lambda x}\right] \tag{A12}$$

$$I_n^4(u) = -\frac{2\lambda}{\pi}\int_{-\infty}^{+\infty}\mathrm{d}x\,\cosh\left(\frac{2\lambda u x}{\pi}\right)\left[\frac{2\cosh x\sinh\left(2\xi/\pi+2n-\lambda-1\right)x}{2\sinh x\cosh\lambda x}\right] \tag{A13}$$

(where $I_n^3(u)$ and $I_n^4(u)$ are related to each other through $\xi \to \pi(\lambda+1)-\xi$). The constant n_* is the number of ν-type poles in the physical strip, which we recall can be written as

$$n_* = \left[\frac{\xi}{\pi} - \frac{1}{2}\right]. \tag{A14}$$

The reflection factors can then be written as

$$-\frac{\mathrm{d}}{\mathrm{d}u}\log\left[\frac{P^+_{|c;\underline{x}\rangle}(u)}{R_0(u)}\right] = I^1(u) + cI^2(u) + \sum_{i\ \mathrm{odd}} I^3_{n_i}(u) + \sum_{j\ \mathrm{even}} I^4_{n_j}(u) \tag{A15}$$

$$-\frac{\mathrm{d}}{\mathrm{d}u}\log\left[\frac{P^-_{|c;\underline{x}\rangle}(u)}{R_0(u)}\right] = I^1(u) - (1-c)I^2(u) + \sum_{i\ \mathrm{odd}} I^3_{n_i}(u) + \sum_{j\ \mathrm{even}} I^4_{n_j}(u) \tag{A16}$$

for topological charge c and $\underline{x} = (n_1, n_2, \ldots, n_{2k+c})$. These factors were given in [7] for the first two levels of excited states (the extent of the spectrum they found); the above is simply a generalization of this to the whole spectrum.

Appendix B. On-shell diagrams

In this appendix we collect together some of the on-shell diagrams used in the main body of the paper. All boundaries are initially in the state $|n_1, n_2, \ldots, n_{2k}\rangle$, where k can be any integer, and we have suppressed the topological charge index (which is zero). Analogous processes for charge 1 states can be found by applying the transformation $\xi \to \pi(\lambda + 1) - \xi$ to all the rapidities shown.

In addition, where the boundary is shown decaying through emission of a breather, only the process where this removes the last two indices is given. Similar processes always exist to remove any other adjacent pair of indices, or to simply modify an index; see section 6.2 for the appropriate breather boundary vertices.

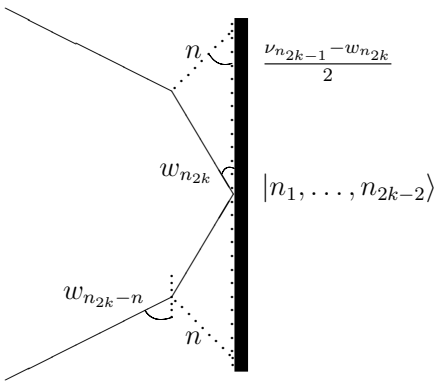

Figure B1. Incoming soliton, breather boundary decay.

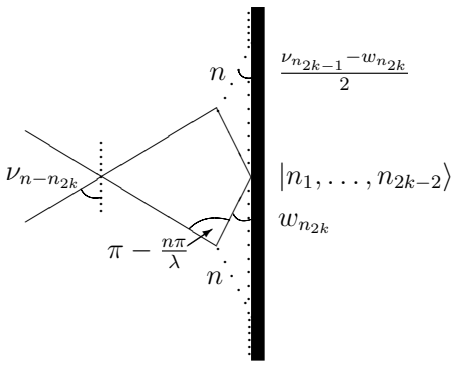

Figure B2. As in figure B1 with incoming soliton crossed.

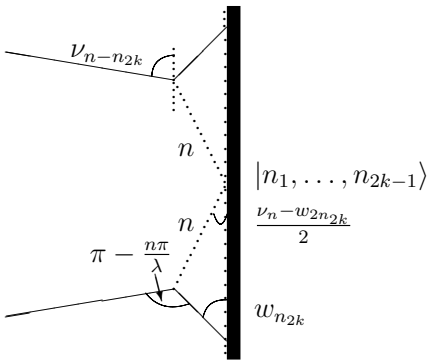

Figure B3. Incoming soliton, soliton boundary decay.

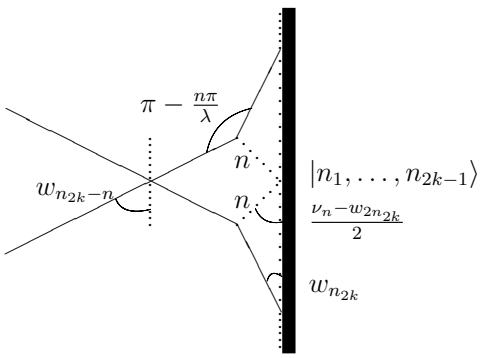

Figure B4. As in figure B3 with incoming soliton crossed.

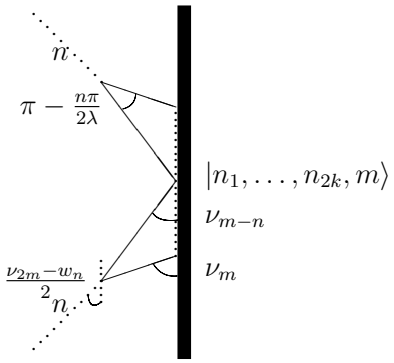

Figure B5. Incoming breather, soliton bound state.

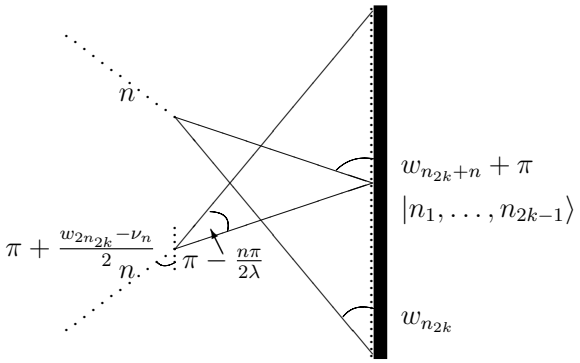

Figure B6. As in figure B5 with outgoing soliton crossed.

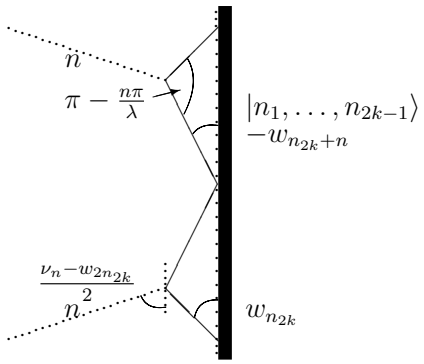

Figure B7. Incoming breather, soliton boundary decay.

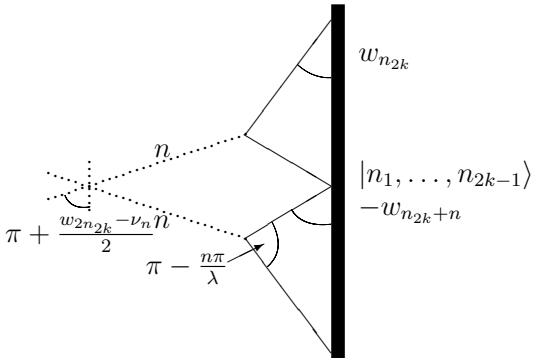

Figure B8. As in figure B7 with incoming breather crossed.

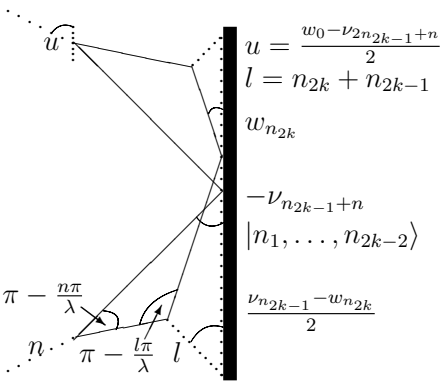

Figure B9. As in figure B5, outer legs replaced by figure B1.

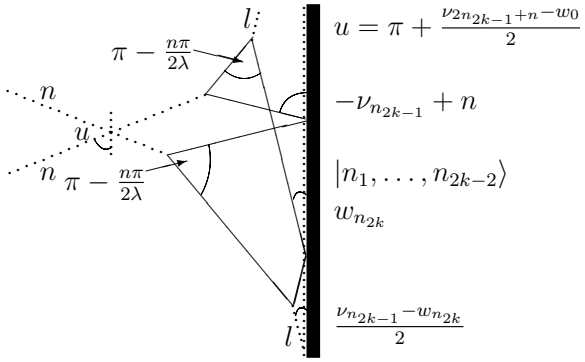

Figure B10. As in figure B8, outer legs replaced by figure B2.

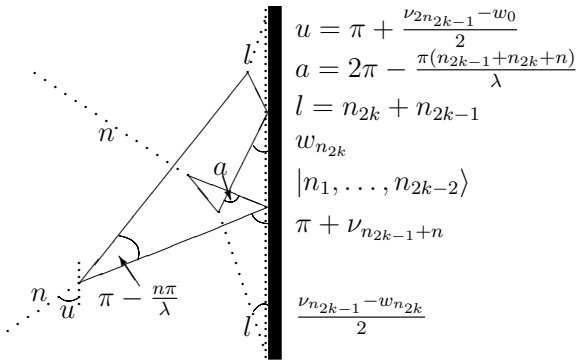

Figure B11. As in figure B6, outer legs replaced by figure B2

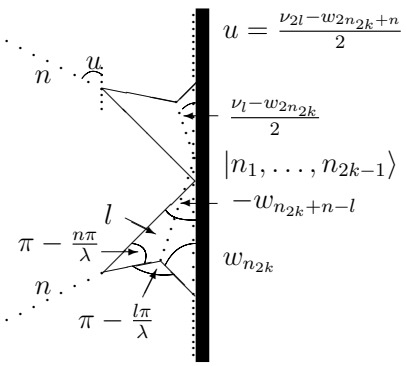

Figure B12. As in figure B5, outer legs replaced by figure B3.

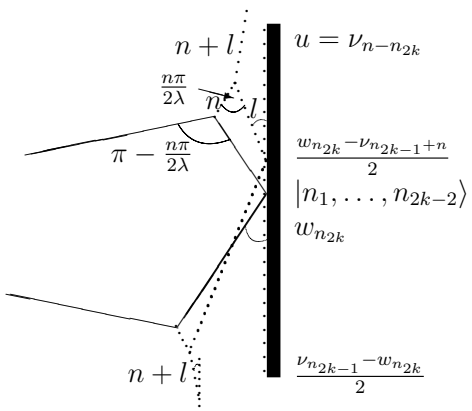

Figure B13. As in figure B2, outer legs replaced by all-breather version.

References

[1] Ghoshal S and Zamolodchikov A 1994 *Int. J. Mod. Phys.* A **9** 3841–85
(Ghoshal S and Zamolodchikov A 1993 *Preprint* hep-th/9306002)
[2] Kane C and Fisher M 1992 *Phys. Rev.* B **46** 15 233–62
[3] Wen X G 1990 *Phys. Rev.* B **41** 12 838–44
[4] Fendley A *et al* 1995 *Phys. Rev. Lett.* **74** 3005–8
(Fendley A *et al* 1994 *Preprint* cond-mat/9408068)
[5] Saleur H 1998 *Preprint* cond-mat/9812110
Saleur H 2000 *Preprint* cond-mat/0007309
[6] Ghoshal S 1994 *Int. J. Mod. Phys.* A **9** 4801–10
(Ghoshal S 1993 *Preprint* hep-th/9310188)
[7] Skorik S and Saleur H 1995 *J. Phys. A: Math. Gen.* **28** 6605–22
(Skorik S and Saleur H 1995 *Preprint* hep-th/9502011)
[8] Dorey P *et al* 1999 *Phys. Lett.* B **448** 249–56
(Dorey P *et al* 1998 *Preprint* hep-th/9810098)
[9] Zamolodchikov A B and Zamolodchikov Al B 1979 *Ann. Phys.* **120** 253–91
[10] Takhtadjian L and Faddeev L 1974 *Theor. Math. Phys.* **21** 160
Korepin V and Faddeev L 1975 *Theor. Math. Phys.* **25** 147
[11] Pillin M 1999 *Phys. Lett.* B **448** 227–33
(Pillin M 1998 *Preprint* hep-th/9812106)
[12] Barnes E W 1901 *Phil. Trans. R. Soc.* A **196** 265–387
Barnes E W 1904 *Trans. Camb. Phil. Soc.* **19** 376–425
[13] Jimbo M and Miwa T 1996 *J. Phys. A: Math. Gen.* **29** 2923–58
(Jimbo M and Miwa T 1996 *Preprint* hep-th/9601135)
[14] Fring A and Köberle R 1994 *Nucl. Phys.* B **421** 159–72
(Fring A and Köberle R 1993 *Preprint* hep-th/9304141)
[15] Coleman S and Thun H J 1978 *Commun. Math. Phys.* **61** 31
[16] Christe P and Mussardo G 1990 *Int. J. Mod. Phys.* A **5** 4581–627
[17] Braden H W *et al* 1990 *Nucl. Phys.* B **338** 689–746
[18] Braden H W *et al* 1991 *Nucl. Phys.* B **356** 469–98
[19] Delius G W *et al* 1992 *Nucl. Phys.* B **382** 365–408
(Delius G W *et al* 1992 *Preprint* hep-th/9201067)
[20] Corrigan E *et al* 1993 *Nucl. Phys.* B **408** 579–99
(Corrigan E *et al* 1993 *Preprint* hep-th/9304065)
[21] Dorey P 1998 *Preprint* hep-th/9810026
[22] Dorey P *et al* 1998 *Nucl. Phys.* B **525** 641–63
(Dorey P *et al* 1997 *Preprint* hep-th/9712197)
[23] Delius G W and Gandenberger G M 1999 *Nucl. Phys.* B **554** 325–64
(Delius G W and Gandenberger G M 1999 *Preprint* hep-th/9904002)